Biophysical Journal Volume 73 October 1997 1742–1762

Configurational Transitions in Fourier Series-Represented DNA Supercoils

Guohua Liu, Tamar Schlick,* Andrew J. Olson, and Wilma K. Olson

Department of Chemistry, Rutgers, the State University of New Jersey, New Brunswick, New Jersey 08903, and *Department of Chemistry and Courant Institute of Mathematical Sciences, Howard Hughes Medical Institute and New York University, New York, New York 10012 USA

ABSTRACT A new Fourier series representation of supercoiled DNA is employed in Langevin dynamics simulations to study large-scale configurational motions of intermediate-length chains. The polymer is modeled as an ideal elastic rod subject to long-range van der Waals' interactions. The van der Waals' term prevents the self-contact of distant chain segments and also mimics attractive forces thought to stabilize the association of closely spaced charged rods. The finite Fourier series-derived polymer formulation is an alternative to the piecewise B-spline curves used in past work to describe the motion of smoothly deformed supercoiled DNA in terms of a limited number of independent variables. This study focuses on two large-scale configurational events: the interconversion between circular and figure-8 forms at a relatively low level of supercoiling, and the transformation between branched and interwound structures at a higher superhelical density.

INTRODUCTION

The comparatively large energetic cost of disrupting the complementary basepair structure gives rise to a unique hierarchy of physical properties in double helical DNA. At chain lengths up to a few helical turns, the molecule resembles a stiff rod with small, almost imperceptible fluctuations of individual chemical residues. In contrast, very long DNA chains adopt compact arrangements compared to the extended regular duplex. At this size range the molecule further qualifies as a random coil in the sense that the distribution of overall three-dimensional spatial arrangements is completely random (Kuhn, 1936, 1939; Flory, 1969). The local structural perturbations accumulate as large-scale configurational changes, leading to all possible dispositions of the polymer ends.

The configurational behavior of DNA between these extremes of chain length is more difficult to characterize (Eisenberg, 1987; Hagerman, 1988; Crothers et al., 1992). State-of-the-art imaging techniques provide intriguing snapshots of a gradually deforming wormlike polymer (Bednar et al., 1995; Hansma et al., 1996; Samori et al., 1996; Lyubchenko and Shlyakhtenko, 1997), revealing the global fluctuations in chain structure. Other new instrumental methods measure the forces that impede the overall deformability of such DNAs (Bensimon et al., 1994; Yin et al., 1995; Bensimon, 1996; Cluzel et al., 1996; Smith et al., 1996; Strick et al., 1996) and image the large-scale molecular movement of the double helix (Perkins et al., 1994; Nie et al., 1995; Volkmuth et al., 1995; Yoshikawa and Matsuzawa, 1995; Samori et al., 1996). Computer simulations can link the local bending, twisting, and stretching of nucleotide residues to global properties of the polymer and thereby complete the current picture of intermediate-length DNA. Representative configurational ensembles obtained from Monte Carlo sampling (Le Bret, 1980; Hagerman, 1985; Levene and Crothers, 1986; Klenin et al., 1991; Zhurkin et al., 1991; Olson et al., 1993; Gebe et al., 1995) uncover details of the global states accessible through thermal fluctuations, while dynamical studies (McCammon and Harvey, 1987; Chirico and Langowski, 1992; Schlick and Olson, 1992a; McConnell et al., 1994; Elcock and McCammon, 1995; York et al., 1995; Cheatham and Kollman, 1996; Sprous and Harvey, 1996; Sprous et al., 1996; Tan et al., 1996; Yang and Pettitt, 1996) give additional insight into the Newtonian pathways of overall structural changes.

The overall flexibility of the double helix is reduced if the chain ends are constrained to fixed positions, as in certain naturally closed circular viruses and plasmids or in protein-anchored DNA loops. Under these conditions, the linking number, or the number of times the two strands of the intact double helix wrap around one another, is conserved. If the linking number is different from the natural intertwining of the two strands in the relaxed, spatially unconstrained linear form (Fuller, 1971, 1978), the chain will supercoil into compact, folded structures. Such plectonemic configurations, typically made up of a central interwound core with sequentially distant segments in intimate contact and two or more sharp hairpin turns, share features of close packing found in crystalline oligonucleotides (Timsit and Moras, 1994, 1995) and tight bending seen in the small DNA loops formed by the binding of various regulatory proteins (Irani et al., 1983; Dunn et al., 1984; Griffith et al., 1986; Ptashne, 1986; Lewis et al., 1996), nucleosomes (Germond et al., 1975; Zivanovic et al., 1988), and recombination complexes

Received for publication 20 December 1996 and in final form 19 May 1997.

Address reprint requests to Wilma K. Olson, Department of Chemistry, Rutgers University, P.O. Box 939 Piscataway, NJ 08855-0939. Tel: 732-445-3993; Fax: 732-445-5958; E-mail: olson@rutchem.rutgers.edu.

This work was taken in part from the dissertation by Guohua Liu written in partial fulfillment of the requirements for the degree of Doctor of Philosophy, Rutgers University, 1996.

0006-3495/97/10/1742/21 $2.00

(Gellert and Nash, 1987; Moitoso de Vargas et al., 1989; Heichman and Johnson, 1990; Kanaar et al., 1990). Because the DNA in most organisms normally exists as supercoiled, the details of these structures and the transitions among different global configurations have attracted considerable attention.

The present work explores the configurational flexibility of intermediate-length supercoiled DNA. The studies are based on Langevin dynamics simulations of a new Fourier series representation of a closed circular chain and an ideal elastic model subject to long-range van der Waals' interactions. The smooth folding of the finite Fourier series-derived double helical axis mimics the wormlike coiling observed in recent physical studies (Boles et al., 1990; Bednar et al., 1995; Hansma et al., 1996; Samori et al., 1996; Lyubchenko and Shlyakhtenko, 1997) and automatically satisfies the ring-closure constraints of cyclic DNA. This new formulation is an alternative to the piecewise B-spline curves used in past work (Hao and Olson, 1989a, b; Schlick and Olson, 1992a) to describe the highly folded pathways of supercoiled DNA in terms of a limited number of independent variables. The Langevin framework incorporates terms to simulate effects of the solvent environment on the closed polymer in the same spirit as the traditional Brownian dynamics methods used by van Waveren et al. (1988) and Chirico and Langowski (1991, 1992, 1994, 1996), as well as the bead-wormlike Brownian dynamics model newly introduced by Jian et al. (1997). The recent molecular dynamics studies of Harvey and co-workers (Sprous and Harvey, 1996; Sprous et al., 1996; Tan et al., 1996), by contrast, focus on the intrinsic molecular motions of supercoiled DNA in the absence of solvent.

Advantages of the Fourier series representation include its accuracy in fitting known data and, as in other curve-fitting techniques, its simplicity in modeling an arbitrary curve (i.e., data compactness). In contrast to the B-spline curves, the independent controlling points of the Fourier-based pathway lie on the curve they define. The elastic model, while primitive in ignoring the sequence-dependent features of the double helix, gives a good first-order approximation of the macroscopic behavior of supercoiled DNA (Olson and Zhang, 1991; Vologodskii et al., 1992; Vologodskii and Cozzarelli, 1994; Olson et al., 1995; Olson, 1996; Schlick, 1995). Unlike conventional all-atom simulations that deduce chain flexibility from the collective motions of the constituent atoms (McConnell et al., 1994; Elcock and McCammon, 1995; York et al., 1995; Cheatham and Kollman, 1996; Yang and Pettitt, 1996), the simplified elastic scheme starts with an assumed conformational behavior of local chain residues. The van der Waals' term prevents the self-contact of distant chain segments while also mimicking attractive forces thought to stabilize the association of closely spaced charged rods at high salt concentrations (Odijk, 1994; Ray and Manning, 1994; Wissenburg et al., 1994). The explicit treatment of long-range electrostatic interactions along the polyelectrolyte backbone, previously incorporated in the B-spline model (Fenley et al., 1994; Schlick et al., 1994b), has not yet been added to the present treatment.

In the following section we introduce the simplified virtual bond model and the Fourier series representation used to describe double helical structure. We then outline the dynamics formalism, the potential energy function used to assess the deformations of the DNA helix, and the time correlation analyses used to classify the different levels of polymer motion. With these tools, we characterize the chain flexibility at both global and local levels. We compare the behavior of the Fourier series-represented curve with that of an equivalent B-spline chain description, and then focus on two large-scale configurational transitions: the interconversion between circular and figure-8 forms at a relatively low level of supercoiling, and that between branched and interwound structures at a higher superhelical density. We end by discussing the advantages and limitations of Fourier series-modeled DNA and outlining the connection between local and global configurational change gleaned from the simulations.

METHODS

DNA model and representation

Conventional all-atom simulations of polymeric DNA are beyond the capabilities of even the most sophisticated current computers. The size and time-limitation problems confronting numerical studies of nucleic acid structure necessitate the use of simple models where the long double helix is approximated by a few points per nucleotide residue. Chains of a few hundred residues are typically described in terms of the rigid body rotations and translations between successive basepair planes (Maroun and Olson, 1988; Tan and Harvey, 1990; Zhurkin et al., 1991; Olson et al., 1993; Marky and Olson, 1994; Olson et al., 1995). The treatment of longer chains entails further simplification to a sequence of virtual bonds, each of which can span several helical turns (Olson, 1979; Klenin et al., 1991). The models of DNA presented below are relatively smooth with virtual bonds linking basepairs separated by slightly less than a complete turn of the double helix. The DNA is further assumed to be inextensible and naturally straight, and to follow ideal elastic behavior with no preferences on the direction of chain bending; as a direct consequence, the twisting deformations are uniformly spread over the polymer in its equilibrium states (Fuller, 1971). The bending constants fit the observed persistence length of DNA (Eisenberg, 1987; Hagerman, 1988; Taylor and Hagerman, 1990). The ease of bending versus twisting, as measured by the ratio of the respective force constants, $\rho = A/C$ (see below), is set arbitrarily to unity, within the biological range (Heath et al., 1996).

The resolution of the captured DNA motions depends on both the length of achievable simulations and the level of chain representation. Large-scale motions of the polymer as a whole become apparent if the chain model is simplified and the number of independent variables is thereby reduced. The extension of the DNA virtual bond unit (with the consequent reduction in the number of such bonds) is justified in short, stiff fragments up to a few helical turns as well as in very long chains, ~2000 basepairs (bp) or more in length according to direct computations of the limiting Gaussian behavior of idealized naturally straight duplexes (Marky and Olson, 1994). Intermediate-length DNA (hundreds of bps) cannot be represented as rigid units since these polymers are quite flexible on the global scale, with mean end-to-end distances appreciably different from the static rod approximation (Zhurkin et al., 1991; Olson et al., 1993). Furthermore, the bending "corrections" needed to relate such rigid segments to the observed persistence length of DNA are exaggerated (Olson et al., 1993; Schellman and Harvey, 1995) and beyond the limited angular range valid for the elastic

approximation. The global folding is also quite irregular in simplified models generated from extended polymer links (Klenin et al., 1991; Chirico and Langowski, 1992). The long stiff segments further prevent the close intertwining of sequentially distant chain fragments observed experimentally (Bednar et al., 1994; Lyubchenko and Shlyakhtenko, 1997).

A finite Fourier series chain representation, by contrast, reduces the number of independent variables in simulations of large-scale polymer mobility while simultaneously mimicking the smooth bending characteristic of intermediate-length DNA. The Fourier coefficients, $\{\mathbf{a}_k\}$ and $\{\mathbf{b}_k\}$ (each a set of three-dimensional vectors), act in concert with controlling points, much like the B-spline controlling points introduced in past work (Hao and Olson, 1989a, b; Schlick and Olson, 1992a), to guide the folding of the double helix axis during the course of computation. The controlling points ($\mathbf{x}_i$, $i = 1, \ldots N$), defined on the smooth Fourier series curve,

$$\mathbf{x}_i = \sum_{k=1}^{N/2} \{\mathbf{a}_k \sin(2\pi k u_i) + \mathbf{b}_k \cos(2\pi k u_i)\} \qquad (1)$$

are more widely spaced ($u_i = 0, \Delta u, 2\Delta u, \ldots, i\Delta u, \ldots, N\Delta u = 0, 1/N, 2/N, \ldots, i/N, \ldots, 1$) than the individual chain units, with their precise locations determined by the contour parameter u ($u = 0, 1/I, 2/I, \ldots, i/I, \ldots, 1$ with $I \ll N$),

$$\mathbf{r}(u) = \sum_{k=1}^{N/2} \{\mathbf{a}_k \sin(2\pi k u) + \mathbf{b}_k \cos(2\pi k u)\}. \qquad (2)$$

As outlined in detail elsewhere (Liu et al., 1995), the controlling points lie along the axis of the DNA duplex and can be fitted to experimentally characterized pathways. The details of local fine structure are incorporated in the mesh parameters. By choosing the appropriate number of mesh points, it is possible to record sequence-dependent secondary structural features (Gorin et al., 1995) using a much smaller number of independent variables. Like the B-spline curves, the Fourier series representation automatically satisfies the ring closure constraint of cyclic DNA and lends itself to systematic studies of macroscopic flexibility. Because the number of independent variables is significantly lower than the number of chain residues, it is possible to simulate the large-scale configurational changes of smoothly deformed supercoiled polymers using such curve-fitting techniques.

Langevin dynamics

The Langevin dynamics formalism with phenomenological terms that mimic environmental forces helps to extend the range of accessible configurations sampled during a simulation (Loncharich et al., 1992; Ramachandran and Schlick, 1995). In the simplest form (i.e., no hydrodynamics), the equations of motion for the independent vector $\mathbf{x} = (x_1, \ldots, x_n)$ are given by

$$\mathbf{M}\frac{d^2\mathbf{x}(t)}{dt^2} = -\nabla E(\mathbf{x}(t)) - \gamma\mathbf{M}\frac{d\mathbf{x}(t)}{dt} + \mathbf{R}(t). \qquad (3)$$

They reflect the simultaneous action of three forces: 1) the systematic internal forces determined by the gradient of the total potential energy, $-\nabla E(\mathbf{x}(t))$; 2) a simple frictional force, $-\gamma\mathbf{M}(d\mathbf{x}(t)/dt)$, due to the relative motions of the polymer through its surroundings (γ is the frictional coefficient); and 3) the imposed random forces, $\mathbf{R}(t)$, that in combination with the other terms establish the thermal reservoir. The random force is modeled as a Gaussian process with a mean of zero and covariance matrix given by:

$$\langle \mathbf{R}(t)\mathbf{R}(t')^{\mathrm{T}} \rangle = 2\gamma k_{\mathrm{B}} T \mathbf{M}\delta(t - t'), \qquad (4)$$

and controlled by γ (which is also called the collision frequency, since it has units of reciprocal time), the Boltzmann constant k_{B}, the temperature T, the collective chain masses in the diagonal matrix $\mathbf{M}$, and the Dirac delta function $\delta(t - t')$, which is one when $t = t'$ and zero otherwise. (The superscript T in Eq. 4 denotes the vector transpose.) The random force, which is uncorrelated with the positions and velocities of chain residues, crudely mimics thermal fluctuations and establishes thermal equilibrium. It compensates for the damping coming from the frictional force. The energy in Langevin simulations is not constant, but rather fluctuates about a mean value that is temperature-dependent.

Integration of the equations of motion (Eq. 3) yields the collective vector of control points, $\mathbf{x}(t)$, at time t. The parameter γ spans the inertial to the diffusive regime and thus governs the nature of global motions of the polymer. The absence of the two added forces (i.e., $\gamma = 0$) corresponds to the molecular dynamics regime wherein the DNA motions are determined by the potential energy gradient (Sprous and Harvey, 1996; Sprous et al., 1996; Tan et al., 1996). The dominance of the random forces at high γ, by contrast, corresponds to the diffusive or Brownian limit measured in hydrodynamic studies of polymeric DNA (Le Bret, 1978; Allison and McCammon, 1984; Chirico and Langowski, 1991, 1996; Matsumoto and Doi, 1994).

For the numerical procedure, we follow the approach previously applied to B-spline representations of idealized supercoiled DNAs (Schlick and Olson, 1992a). In each time step, the new configuration, $\mathbf{x}^{n+1}$, is obtained by minimizing the "dynamics function,"

$$\Phi(\mathbf{x}) = \tfrac{1}{2}(1 + \gamma\Delta t)(\mathbf{x} - \mathbf{x}_0^n)^{\mathrm{T}}\mathbf{M}(\mathbf{x} - \mathbf{x}_0^n) + \Delta t^2 E(\mathbf{x}), \qquad (5)$$

where

$$\mathbf{x}_0^n = \mathbf{x}^n + \frac{\Delta t}{1 + \gamma\Delta t}(\mathbf{v}^n + \Delta t\mathbf{M}^{-1}\mathbf{R}^{n+1}) \qquad (6)$$

is known from the coordinates $\mathbf{x}^n$ and velocities $\mathbf{v}^n$ calculated at time step n, and the random force $\mathbf{R}^{n+1}$ is chosen independently at step $n + 1$. The starting point for minimization can be taken as $\mathbf{x}^n$, and the new velocity is computed from the finite difference $\mathbf{v}^n = (\mathbf{x}^{n+1} - \mathbf{x}^n)/\Delta t$. The minimization at each step is performed here using the truncated-Newton method (Schlick and Fogelson, 1992a, b) adapted for the Fourier series model (Liu et al., 1995).

As demonstrated in previous Monte Carlo (Zhang et al., 1991, 1994) and energy minimization (Liu et al., 1995) studies of Fourier series-represented supercoiled DNA, it is more convenient to use the Fourier coefficients than the curve points as computational variables. Here we prove that minimization of the dynamics function, $\Phi(\mathbf{x})$, in terms of the Fourier coefficients is equivalent to minimization with respect to the controlling points. Thus, we can take advantage of previously reported derivatives (Liu et al., 1995) in evaluating the gradient and Hessian of $\Phi(\mathbf{x})$ with respect to the Fourier coefficients.

To minimize $\Phi(\mathbf{x})$ with respect to the controlling points, the equations $\partial\Phi(\mathbf{x})/\partial\mathbf{x}_i = 0$, $i = 1, N$ must be solved. If $\mathbf{y}_k$ denotes a Fourier coefficient (i.e., $\mathbf{a}_k$ or $\mathbf{b}_k$ in Eqs. 1 and 2), then from Fourier analysis, we know that $\mathbf{y}_k$ is a function of $\mathbf{x}_i$ (i.e., $\mathbf{y}_k = \mathbf{y}(\mathbf{x}_i)$, $k = 1, N$, $i = 1, N$) or conversely $\mathbf{x}_i$ is a function of $\mathbf{y}_k$ (i.e., $\mathbf{x}_i = \mathbf{x}(\mathbf{y}_k)$). Hence, by the chain rule,

$$\frac{\partial\Phi(\mathbf{x})}{\partial\mathbf{x}_i} = \sum_{k=1}^{N} \frac{\partial\Phi(\mathbf{x}(\mathbf{y}_k))}{\partial\mathbf{y}_k}\frac{\partial\mathbf{y}_k}{\partial\mathbf{x}_i}, \qquad (7)$$

Thus, if $\partial\Phi(\mathbf{x}(y_k))/\partial\mathbf{y}_k = 0$, $k = 1, N$, then $\partial\Phi(\mathbf{x})/\partial\mathbf{x}_i = 0$ for $i = 1, N$, and the minimization of $\Phi(\mathbf{x})$ against controlling points or Fourier coefficients is equivalent.

The gradient and Hessian of $\Phi(\mathbf{x})$ with respect to Fourier coefficient $\mathbf{y}_k$ are obtained by rewriting Eq. 5 as:

$$\Phi(\mathbf{x}(\mathbf{y})) = \tfrac{1}{2}(1 + \gamma\Delta t)(\mathbf{x}(\mathbf{y}) - \mathbf{x}_0^n)^{\mathrm{T}}\mathbf{M}(\mathbf{x}(\mathbf{y}) - \mathbf{x}_0^n) + \Delta t^2 E(\mathbf{x}(\mathbf{y})). \qquad (8)$$

Here $\mathbf{y} = \{\mathbf{a}_1, \mathbf{b}_1, \mathbf{a}_2, \mathbf{b}_2, \ldots, \mathbf{a}_{k/2}, \mathbf{b}_{k/2}\}$, and the equation of the DNA curve (Eq. 2) is expressed as:

$$\mathbf{x}(u) = \begin{bmatrix} x_1(u) \\ x_2(u) \\ x_3(u) \end{bmatrix} = \sum_{k=1}^{N} \mathbf{y}_k F_k(u), \tag{9}$$

with $F_k(u) = \sin(2\pi ku)$ for odd k, $F_k(u) = \cos(2\pi ku)$ for even k, $\mathbf{y}_k = \{y_{k1}, y_{k2}, y_{k3}\}$. It follows that

$$\frac{\partial \Phi(\mathbf{x}(\mathbf{y}))}{\partial y_{kl}} = \left(\frac{\partial \Phi(\mathbf{x})}{\partial \mathbf{x}}\right)\left(\frac{\partial \mathbf{x}}{\partial y_{kl}}\right) = \sum_{i=1}^{N'} (1 + \gamma \Delta t) m_i F_k(u_i) + \Delta t^2 \left(\frac{\partial E(\mathbf{y})}{\partial y_{kl}}\right), \tag{10}$$

and

$$\frac{\partial \Phi^2(\mathbf{x}(\mathbf{y}))}{\partial y_{kl} \partial y_{jn}} = \sum_{i=1}^{N'} \delta_{ln}(1 + \gamma \Delta t) m_i F_k(u_i) F_j(u_i) + \Delta t^2 \left(\frac{\partial E^2(\mathbf{y})}{\partial y_{kl} \partial y_{jn}}\right), \tag{11}$$

where m_i is the mass of controlling point i, δ_{ln} is the Kroneker delta, and $l = 1, 3$. The $[\partial E(\mathbf{y})/\partial y_{kl}]$ term and the part of $[\partial E^2(\mathbf{y})/\partial y_{kl} \partial y_{jn}]$ which is used as the preconditioner for energy minimization are expressions detailed previously (Liu et al., 1995).

Potential energy function

The potential function determining the internal forces of the DNA is a composite of several terms. Harmonic bending, twisting, and stretching contributions limit the deformations of the chain from its ideal, naturally straight B-DNA reference state, while a van der Waals' term mimics the interactions of distant parts of the polymer. Conformational changes to other secondary structural forms (e.g., A-DNA, melted states, etc.) are not considered.

The bending term,

$$E_{\text{Bend}} = \frac{A}{2} \sum_{i=1}^{N} \kappa_i^2 \Delta s, \tag{12}$$

is parameterized (Landau and Lifshitz, 1980) through the force constant, $A = ak_BT = 2k_BT\Delta s/\langle \Delta\theta^2 \rangle$, to reproduce the mean-square bending angle per residue, $\langle \Delta\theta^2 \rangle$, consistent with the observed persistence length of DNA, a, and the assumed distance between chain units, Δs. Like the other terms discussed below, the bending energy is computed at the level of virtual bonds (i.e., mesh points along the chain contour) rather than at the level of the controlling points (i.e., Fourier coefficients) used to define global configuration. As detailed elsewhere (Schlick and Olson, 1992a; Liu et al., 1995), a finer grid of energy terms is incorporated in the derivatives used to solve the dynamics function (Eq. 5) that guides the course of the simulation. In this sense, the local character of the DNA is incorporated in the simulations of global chain motions.

The twisting expression,

$$E_{\text{Twist}} = \frac{2\pi^2 C}{L_0} (\Delta Lk - Wr)^2, \tag{13}$$

is an approximation that assumes that the dispersion in the twist density of the repeating steps along the contour of a given chain configuration, $\langle \Delta\omega^2 \rangle^{1/2} = (\langle \omega^2 \rangle - \langle \omega \rangle^2)^{1/2}$, is small compared to the deviation between the mean and intrinsic twisting of the residues, $(\langle \omega \rangle - \omega_0)$. Currently, there are no good estimates of the likely magnitude of the twist dispersion along the contour of a nonequilibrium DNA structure and of its dependence on global configuration and external forces. The twist density is assumed, for simplicity, to be uniform and the dispersion to be null as in the equilibrium states of an ideal elastic rod (Zajac, 1962; Fuller, 1971; Le Bret, 1984). As Gebe et. al. (1995) have recently pointed out, the writhing number, Wr, and the linking number difference, ΔLk, appearing in Eq. 13 are related under these conditions by White's equation (1969) to the difference between $\langle \omega \rangle$ and ω_0. The writhing number is a standard measure of global folding defined in terms of the distances and orientations of the constituent chain segments (White, 1989), while the linking number is the number of times the two strands of the closed double helix wrap around each other. The twisting energy is thus determined by the pathway of the DNA axis, the degree of supercoiling as measured by the difference, $\Delta Lk = Lk - Lk_0$, between the imposed and natural linking numbers, and the twisting force constant, C. The computational advantages of omitting individual basepairs in this treatment are obvious. Potential errors arising with this approximation are discussed below in terms of the observed configurational behavior.

The stretching contribution,

$$E_{\text{Stretch}} = K(L(\mathbf{x}) - L_o)^2, \tag{14}$$

is a computational device introduced to restrain the total contour length of the DNA to its equilibrium value so that the chain behaves like an inextensible elastic rod. The choice of the force constant, K, in this expression ensures that the contributions of E_{Stretch} to the total energy are negligible.

The van der Waals' energy,

$$E_{\text{vdW}} = -\epsilon \left[\left(\frac{d}{d_{ij}}\right)^{12} - 2\left(\frac{d}{d_{ij}}\right)^{6} \right], \tag{15}$$

is designed to produce an energy minimum of magnitude ϵ when d_{ij}, the spatial separation of segments i and j, which are far from one another along the chain contour, equals d. The dominance of the repulsive term at shorter distances prevents chain crossings, while the attractive term mimics stabilizing forces identified in recent theoretical studies of closely spaced charged rods (Odijk, 1994; Ray and Manning, 1994). These interactions, which are thought to reflect the shared counterion atmosphere of the rods (Ray and Manning, 1994), help rationalize the spontaneous aggregation of short DNA fragments at 1 M NaCl (Wissenburg et al., 1994). Favorable dispersion forces also account for the collapse in T7 bacteriophage structure brought about by multivalent counterions (Bloomfield et al., 1980).

Correlation analyses

The global motions of the supercoiled DNA are monitored using a time correlation analysis of selected geometrical parameters. The global orientation of the chain is measured in terms of the directions of the three principal axes ($\boldsymbol{\rho}_1, \boldsymbol{\rho}_2, \boldsymbol{\rho}_3$) of the radius of gyration, while the shape of the DNA is characterized by the root-mean-square moments (I_1, I_2, I_3) along each of the axes; see Yevich and Olson (1979), Schlick and Olson (1992a), and Marky and Olson (1994) for computational details. The rate of end-over-end tumbling is determined from the angle, $\phi_1(\tau)$, between the largest principal axis at different time intervals, τ, during the course of the dynamics simulation, while the rates of global rotation about the long axis are obtained from the corresponding angles, $\phi_2(\tau)$ and $\phi_3(\tau)$, between the two smaller principal axes. The frequency of collective chain bending is examined in terms of the writhing number, Wr, and the changes in local bending are assessed from the variation in residue bending angles, $\Delta\theta_p = \kappa_p \Delta s$, at representative points p along the chain contour.

The autocorrelation functions for most of the dynamical variables (i.e., Wr, I_i, $\Delta\theta_p$) are obtained in the standard fashion (Chandler, 1987) by evaluating the mean product of the instantaneous deviation of a given variable, V, at time step t from its equilibrium average, $\langle V \rangle$, and its spontaneous fluctuation at time $t + \tau$. To facilitate comparison of the time-dependent behavior at the local and global levels, the data are nor-

malized with respect to the dispersion of V, evaluated over the same time set,

$$C_V(\tau) = \frac{\langle (V(t+\tau) - \langle V \rangle)(V(t) - \langle V \rangle) \rangle}{\langle (V(t) - \langle V \rangle)^2 \rangle}. \quad (16)$$

The equilibrium average, $\langle V \rangle$, is evaluated over all time steps, while the time-dependent terms embedded in this expression—$\langle V(t) \rangle$, $\langle V(t+\tau) \rangle$, and $\langle V(t+\tau)V(t) \rangle$—are determined over the range in the given time interval. To reduce statistical errors due to insufficient sampling, the maximum value of τ is taken to be half the number of iteration steps in the simulation. The relative frequencies of the different chain motions become apparent when the $C_V(\tau)$ are plotted versus τ.

The time correlation functions used to monitor chain tumbling and rotation, $C_{\cos\phi_i}(\tau)$, are defined somewhat differently in terms of the scalar products of the three principal axes at iterations t and $t+\tau$,

$$C_{\cos\phi_i}(\tau) = \frac{1}{T'} \sum_{t=1}^{T'} \boldsymbol{\rho}_i(t) \cdot \boldsymbol{\rho}_i(t+\tau) = \frac{1}{T'} \sum_{t=1}^{T'} \cos \phi_i(t,(t+\tau)). \quad (17)$$

The index t in this expression corresponds to a given step during the dynamics simulation, while T' is the total number of pairs of iteration steps separated by time interval τ (not to be confused with the temperature T in Eq. 4).

Computations

Simulations were performed on a Silicon Graphics Indigo II Extreme computer at Rutgers University and on a faster Silicon Graphics Power Challenge R10,000 processor at New York University. Simulations of 20,000 steps require 48 CPU hours (for the Fourier series representation) on the former and 18 CPU hours (for B-splines) on the latter. At the optimal γ where the physical times corresponds to 200 μs, the performance of the two approaches is ~4.2 and 11 μs/CPU-h, respectively. A reference figure from the Brownian dynamics simulations of Chirico and Langowski (1996) for a polygonal chain model with roughly three times the number of independent variables is 1.75 μs/CPU-h on a 150-MHz Silicon Graphics Indy R4400 (which has the same processor as the Indigo II Extreme). However, there are undoubtedly many differences in implementation and levels of program optimization. The advantages of curve-fitting techniques like Fourier series representations and B-splines are not only data compactness, which is important for long dynamic runs, but also the capability to link global and local structural deformations (see below).

Settings

We simulate a 1000 bp (3400 Å) elastic DNA chain at a temperature of 300 K subject to different levels of supercoiling. Positive values of ΔLk are chosen in order to compare the simulations with earlier work (Schlick and Olson, 1992a, b; Schlick et al., 1994c). The configurations of negatively supercoiled DNA found in naturally occurring systems are simply the mirror images of those reported below. The curve of the DNA model is represented by 16 evenly spaced controlling points, or equivalently by 16 Fourier coefficients. For simplicity, the masses of the controlling points are set to unity (1 g/mol) (Schlick and Olson, 1992a). This assignment scales the program time step (100 fs) by a factor $\alpha = (m/m')^{1/2}$, where m' is the program mass and m the corresponding physical mass, yielding a program time step of ~20 ps in the dynamics simulation (Schlick et al., 1994a; Ramachandran and Schlick, 1996). (We take the mass per basepair to be 660 amu so that α is 203, i.e., $(6.6 \times 10^5/16)^{1/2}$). The physical time scale of the simulations thus depends on m' and γ (see below); the optimal sampling γ is 700 times lower than the experimentally relevant value, resulting in an effective time step of ~10 ns in the diffusive regime (based on the calibration of simulated values with measured translational diffusion constants) (Ramachandran and Schlick, 1996).

The mesh parameter in Eq. 2 is set to 7 so that a total of 112 points, each corresponding to a virtual bond ~9 bp in length, is used for the computation of energy terms and chain dimensions. The energy parameters are identical to those used previously in the energy minimization of the Fourier series-represented chain (Liu et al., 1995): A = 331.2 (kcal/mol)Å, corresponding to a persistence length of 561 Å; $\rho = A/C = 1$, corresponding to $A = C = 2.32 \times 10^{-19}$ erg-cm at 300 K; K = 0.5 kcal/mol-Å^2; $\epsilon = -0.05$ kcal/mol; and d = 30 Å, corresponding to the diameter of the hydrated double helix (Podgornik et al., 1995). A physical stretching term consistent with recent DNA-pulling experiments (Bensimon et al., 1994; Yin et al., 1995; Bensimon, 1996; Cluzel et al., 1996; Smith et al., 1996; Strick et al., 1996) can be incorporated in the future. Stretching, however, is known to be of secondary importance in equilibrium studies of supercoiled molecules (Westcott, 1996; Westcott et al., 1997).

In practice, a Fourier fitting is performed at each iteration of dynamics to generate the coordinates of the controlling points introduced in the "constant" ($\mathbf{x}_0^n$) of the dynamics function, $\Phi(\mathbf{x})$ (Eqs. 5 and 6). Two to three outer iterations generally suffice to minimize $\Phi(\mathbf{x})$ and thereby to make the next configurational move. The trajectories are initialized with all energy terms chosen to be kinetic by independently choosing each component of the initial velocity from a Gaussian distribution centered at zero with variance k_BT. The sum of all components of the velocity, $\frac{1}{2}(\mathbf{v}^0)^T\mathbf{M}(\mathbf{v}^0)$, will then be normally distributed and equal to $3Nk_BT$. The components of the random force at controlling point i are similarly selected at each iteration from a fixed Gaussian distribution centered at zero with variance $2\gamma k_BTm_i\Delta t$ so that Eq. 4 is satisfied. The damping constant, γ, is chosen below after examining the global behavior of the chain in simulations carried out at representative values.

RESULTS

Local and global motions

The parameter γ in the phenomenological Langevin equation can be chosen so as to reproduce the experimentally observed translational diffusion constant for the modeled system. This is possible because the value derived from Langevin simulations in the diffusive regime (from the mean-square fluctuations of the center-of-mass position, according to the Einstein-Stokes equation) is $k_BT/\gamma\Sigma m$, where the sum in the denominator corresponds to the total mass of the simulated system. According to Ramachandran and Schlick (1996), the physically relevant γ value for closed-circular DNA lies in the range of 10^{11} s^{-1}. However, it is well known that, because of the sampling problem, a computationally optimal γ can be much smaller in Langevin simulations. For example, Pastor and co-workers (Loncharich et al., 1992) use $\gamma = 2$ ps^{-1} for peptides to maximize sampling of isomerization events and hence obtain better statistics; this value is smaller by an order of magnitude than γ = 50–60 ps^{-1}, the typical collision frequency for protein atoms exposed to solvent with a viscosity of 1 cp. In the diffusive regime (large γ limit), scaling of time-dependent quantities can be done in correspondence with scaling γ. This is because the friction, and hence the relaxation time, is proportional to the viscosity. Thus, using a smaller γ than relevant physically corresponds to scaling the characteristic times.

In this work, we use two values of γ corresponding to the moderate and high-damping regimes: 10^{11} and 10^{13} s^{-1}, in program units. Using the mass scaling factor α = 203, these values correspond to ~5×10^8 and 5×10^{10} s^{-1}, respec-

tively (Ramachandran and Schlick, 1996). The latter value is thus close to the value determined above on the basis of the experimental translational diffusion constant. To compare with available estimates of the relaxation time of the writhing number, we show in Fig. 1 *B* the normalized autocorrelation functions of the writhing number for closed circular 1000-bp DNA for these two γ values at $\Delta Lk = 4.0$, a linking number difference corresponding in magnitude to typical physiological levels of supercoiling (Bauer, 1978). The relaxation time of $\sim$1000 iterations for the larger γ value agrees with the microsecond time for relaxation of Chirico and Langowski (1996) and of Jian (1997) in combination with our time step estimate in the nanosecond range (Ramachandran and Schlick, 1996). The explicit incorporation of hydrodynamic effects in the other works presumably accounts for the absence of any of the oscillatory motion seen here. Increasing γ in our framework has the same effect (Fig. 1 *B*).

Figs. 1 *C* and 1 *D* show autocorrelation functions for I_i, the principal moment of the radius of gyration and $\Delta\theta_p$, selected bending angles along the DNA contour. Fig. 1 *A* follows the time course of end-over-end tumbling measured by the autocorrelation of the mean scalar product between long axes of different chain configurations. Molecular images from these simulations are shown in Fig. 2 *A* and *B* and mean values and corresponding standard deviations (σ) of the geometric parameters and energy terms are reported in Table 1. Note from Fig. 1 *B* that the fluctuations of *Wr* at the larger γ are closely linked to those of $\Delta\theta_4$, the stiffest and straightest of the representative bend angles located in the interwound core of the supercoiled polymer (Table 1). (The periodicity in the writhing number at the smaller γ is also tied to $\Delta\theta_4$.) The linear correlation coefficient between corresponding $C_{Wr}(\tau)$ and $C_{\Delta\theta_4}(\tau)$ values in Fig. 1 *B* and *D* is 0.77. The first and second principal moments at higher γ (Fig. 1 *C*), by contrast, exhibit a different pattern of change which closely matches the long-time periodicity of $\Delta\theta_6$ and $\Delta\theta_8$, two of the most highly deformable angles. Regular variations in the latter parameters alternately extend and shorten the length of the interwound contact zone at the expense of tightening or opening the hairpin loops at the extreme "ends" of the elongated DNA supercoil. (The autocorrelations of I_1 and I_2 at the smaller γ are similarly coupled to changes in angles of high mean bending and flexibility, most notably those in $\Delta\theta_1$ and $\Delta\theta_6$ illustrated in Fig. 1 *D*). There is no apparent relation between changes in molecular configuration and the collective spinning of the chain about its long axis measured by $C_{\cos\phi_1}$ (Fig. 1 *A*), as all global motion is affected strongly by the imposed solvent.

Comparison with B-spline modeling

Configurational characteristics

A 1000-bp supercoiled DNA modeled by the energy terms and dynamics scheme outlined above but described in terms of piecewise smooth cubic B-spline curves exhibits qualitatively similar behavior to that found with the finite Fourier series representation. The two sets of chain configurations described in the legend to Fig. 3 were collected over the same time interval (20,000 iterations) in simulations starting from the respective $\Delta Lk = 4$ minimum energy states with the smaller γ value. The same local structural detail was used: 112 virtual bonds for the 16 B-spline controlling points with a local 7-point mesh, and the 16 Fourier controlling points/coefficients with a 7-point mesh. Both simulations span a wide range of configurations, although the distribution of *Wr* associated with the Fourier series-represented chain is skewed to higher values than that found with the B-spline curves (Fig. 3). These differences are also reflected in the mean values of *Wr*, 2.9 $\pm$ 0.3 for the set of B-spline curves versus 3.1 $\pm$ 0.3 for the finite Fourier series. Because of these differences, the twisting energy is lower on average for the Fourier series data (1.7 $\pm$ 1.2 kcal/mol) than for the B-spline configurations (2.7 $\pm$ 1.3 kcal/mol). Both sets of data roughly match the corresponding Gaussian distributions described by the respective average and mean-square writhing numbers. The root-mean-square deviations between the idealized curves and histograms in Fig. 3 are 7.7% for the Fourier series data and 9.3% for the B-spline sample.

The Fourier series configurations are also less severely bent on average than the B-spline curves ($\langle E_{\text{Bend}}\rangle$ = 13.6 $\pm$ 1.5 versus 14.3 $\pm$ 1.7 kcal/mol), and more favorably packed in terms of mean van der Waals' interactions ($\langle E_{\text{vdW}}\rangle$ = -5.6 ± 0.7 versus -4.4 ± 0.9 kcal/mol). The mean total energy of the finite Fourier series sample (9.7 $\pm$ 1.9 kcal/mol) is thus considerably lower than that of the B-spline data set (12.6 $\pm$ 1.9 kcal/mol). As noted previously (Liu et al., 1995), a higher value of *Wr* and a lower total energy are consistently found upon minimization of a Fourier series-represented chain compared to a B-spline curve under the same computational conditions. The writhing numbers of the minimized $\Delta Lk = 4$ starting states used in the present simulations are 3.4 for the Fourier series curves and 3.1 for the B-spline data with respective total potential energies of 3.7 and 6.3 kcal/mol.

Distinctions of chain representation

The observed differences between the two data sets reflect both the global nature of the Fourier series pathway and its different control compared to the B-spline curves. The variation of one of the Fourier controlling points alters the shape of the whole curve, whereas a given B-spline point affects the configuration locally. Furthermore, because the B-spline controlling points guide, but do not fall, along the curves they determine (Gordon and Riesenfeld, 1974), the fine tuning of overall shape may be difficult. Their influence on local features of the curve is not uniform with the result that the variation of one of these parameters does not necessarily translate into proportional changes in the mesh points used to assess the energy. By contrast, it is easier to optimize local bending and long-range contacts in terms of represen-

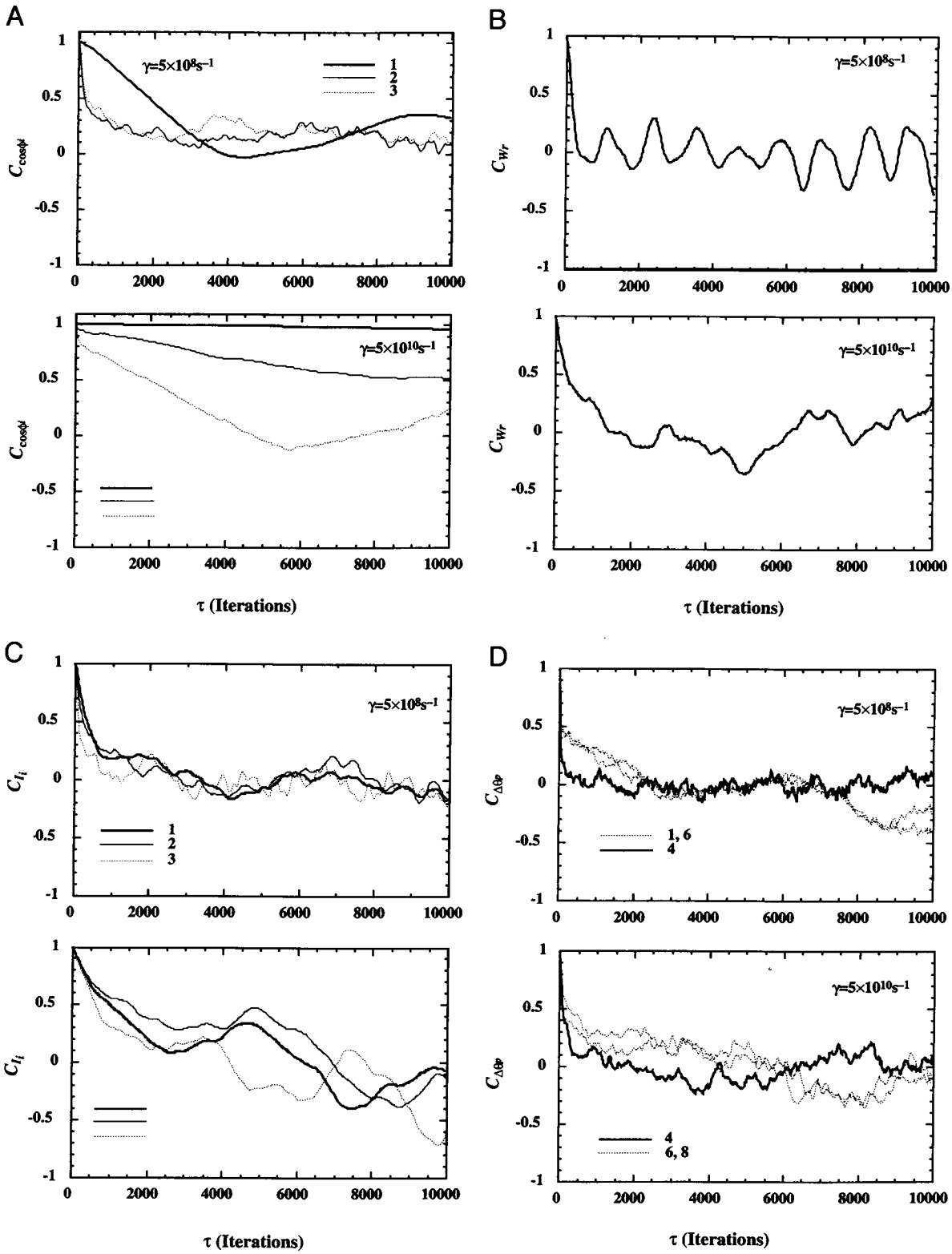

FIGURE 1 Time correlation functions of selected geometric parameters characterizing the DNA configurations from the Langevin dynamics simulations of a 1000-bp Fourier series-represented DNA supercoil. Calculations performed with $\Delta Lk = 4.0$ starting from the interwound equilibrium configuration detailed in Table 1. Each iteration corresponds to a program time step of 100 fs, which is associated with a physical time step of order ns (see text). Each set of plots illustrates the effect of the damping constant, γ, given in physical units: (*A*) $C_{\cos\phi_i}$, the time average of $\cos\phi_i$, where ϕ_i is the angle between the *i*th principal axes of configurations separated by a given time interval, τ. See text for computational details and discussion; (*B*) C_{Wr}, the normalized autocorrelation of the writhing number of states separated by the given time interval; (*C*) C_{Ii}, the normalized autocorrelation of the specified principal moment of the radius of gyration versus time increment; (*D*) $C_{\Delta\theta_p}$, the normalized autocorrelation function of the angle, $\Delta\theta_p$, located on the DNA curve at a fractional distance, $p/10$, along the total contour of the chain; here $p = 1$, 4, 6, and 8.

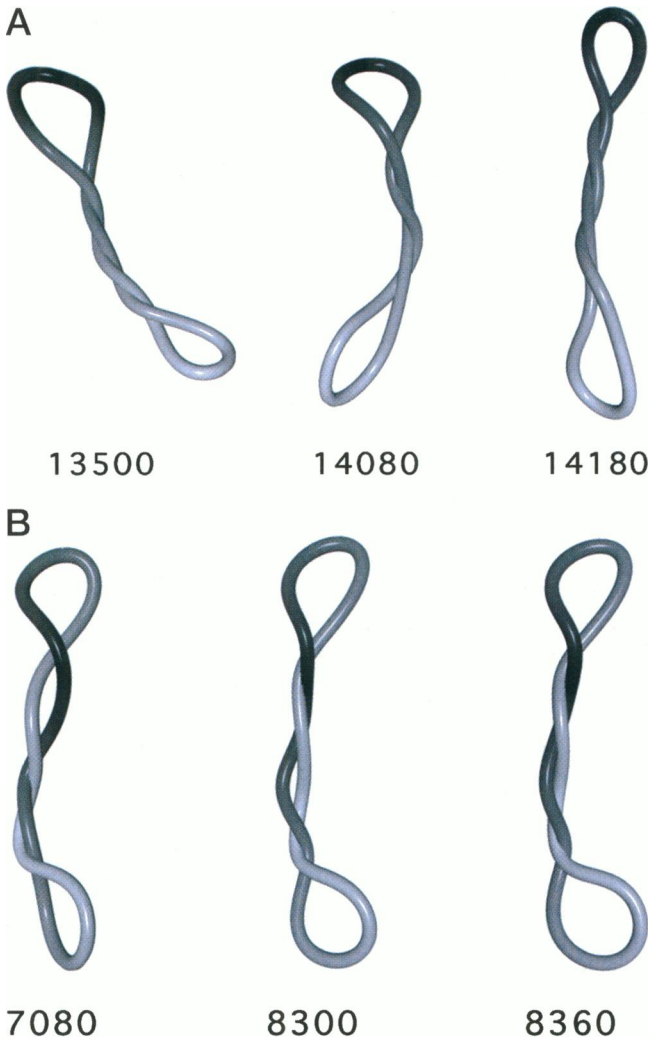

FIGURE 2 Molecular images of representative configurations sampled in the Langevin dynamics simulations of supercoiled DNA subject to the solvent conditions in Fig. 1: (*A*) iterations 13,500, 14,080, and 14,180 representative of the variation in Wr (with respective values of 4.2, 3.0, 3.3) observed at the lower γ; (*B*) iterations 7080, 8300, and 8360 illustrative of the range of total energies (E = 19.6, 29.4, and 28.0 kcal/mol, respectively) sampled at the higher γ. The arc length-dependent shading of the closed curves suggests to the absence of slithering motions (i.e., movement of parts of the chain past one another) over the designated time intervals.

tative Fourier controlling points that lie on the curve they define. The local mesh accordingly varies more uniformly with a change of controlling point.

Energetic approximations

Despite the wide sampling of configuration space in these simulations, the local bending of the DNA model is highly restricted compared to its expected variation. The choice of bending constant corresponds to root-mean-square bending deformations of ~19° at 300 K between the 112 virtual bond segments. An isolated bend of this magnitude will raise the energy of the elastic rod by k_BT (Landau and Lifshitz, 1980). The root-mean-square bend angles found at

TABLE 1 Comparative geometric and energetic parameters found in Langevin dynamics simulations of Fourier series-represented supercoiled DNA chains subject to different damping constants, γ, given in physical units

	$\gamma = 5 \times 10^8$ s^{-1}	$\gamma = 5 \times 10^{10}$ s^{-1}	Energy Minimum
$\langle Wr \rangle$	3.1 (0.3)	3.4 (0.1)	3.4
$\langle I_1 \rangle$	392 (49)	410 (17)	458
$\langle I_2 \rangle$	111 (28)	87 (14)	52
$\langle I_3 \rangle$	59 (16)	56 (11)	51
$\langle E_{Twist} \rangle$	1.7 (1.2)	0.7 (0.3)	0.7
$\langle E_{Bend} \rangle$	13.6 (1.5)	16.8 (1.6)	10.7
$\langle E_{vdW} \rangle$	−5.6 (0.7)	−3.3 (1.2)	−7.8
$\langle E \rangle$	9.7 (1.9)	14.2 (2.3)	3.6
$\langle \Delta\theta_1 \rangle$	6.8 (2.7)	7.9 (2.5)	5.4
$\langle \Delta\theta_2 \rangle$	5.1 (3.1)	9.4 (3.1)	10.2
$\langle \Delta\theta_3 \rangle$	4.1 (2.1)	4.2 (2.3)	1.5
$\langle \Delta\theta_4 \rangle$	4.2 (2.1)	4.1 (2.1)	2.0
$\langle \Delta\theta_5 \rangle$	7.8 (3.2)	6.1 (2.7)	4.0
$\langle \Delta\theta_6 \rangle$	7.0 (2.8)	8.6 (3.1)	5.4
$\langle \Delta\theta_7 \rangle$	5.5 (2.8)	8.9 (2.9)	10.2
$\langle \Delta\theta_8 \rangle$	4.0 (2.1)	4.7 (2.7)	1.5
$\langle \Delta\theta_9 \rangle$	4.2 (2.1)	5.5 (2.5)	2.0
$\langle \Delta\theta_{10} \rangle$	7.8 (3.2)	5.3 (2.8)	4.1

The units of energy are kcal/mol, those of the principal moments (I_1, I_2, I_3) Ångstroms, and those of the bending angles (θ_p, p = 1,10) degrees. Average values and standard deviations (in parentheses) are compared with the corresponding parameters for the minimum energy configuration at ΔLk = 4, the linking number difference used in the simulations.

representative points along the Fourier series curves, $\langle \Delta\theta \rangle^{1/2} = \{\langle \Delta\theta \rangle^2 + [(N-1)/N]\sigma^2_{\Delta\theta}\}^{1/2}$, however, are less than half this value (4.1–9.4° at the larger γ in Table 1). Monte Carlo

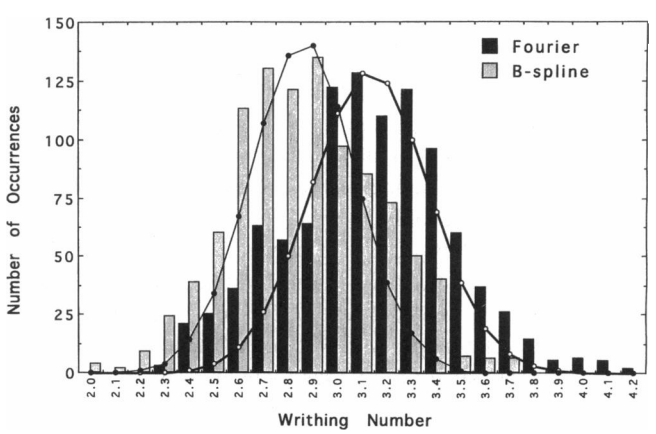

FIGURE 3 Distributions of the writhing numbers of B-spline and Fourier series-represented DNA chain configurations collected over the same time interval (20,000 iterations) in Langevin dynamics simulations starting from the respective ΔLk = 4 minimum energy states with the lower γ. Computations were carried out at the same level of structural detail—a 112 virtual bond representation generated, respectively, with 16 B-spline controlling points and a local 7-point mesh or 16 Fourier controlling points/coefficients and a 7-point mesh. Histograms of simulated occurrences are compared with ideal Gaussian curves, $W = W_0 exp[-(Wr - \langle Wr \rangle)^2/2\langle \Delta Wr^2 \rangle]$, where $\langle Wr \rangle$ is the average writhing number over the respective configurational samples, $\langle \Delta Wr^2 \rangle$ is the mean-square fluctuation of the writhing number, and W_0 is a normalizing factor chosen so that the curves and histograms coincide in the range of maximum occurrences.

simulations, by contrast, easily sample the desired range of local residue bending with simple adjustment of configurational step size (Klenin et al., 1991), but offer no information on the ease of structural transitions. The sampling of local conformation space (i.e., residue bending) in the current dynamics protocol is determined by a combination of many factors, including the governing potential function and the choice of independent structural parameters. The dramatic change in configurational profiles found upon incorporation of torsional forces in recent Brownian dynamics simulations of DNA supercoils (Chirico, 1996) suggests that the local conformation may be affected by the twisting energy. The omission here of energetic contributions arising from the instantaneous deviations of the twist at individual residues, $(C/2)\ (\omega_i - \langle\omega\rangle)^2$, may account for the limited range of local chain bending that is observed. New computational approaches that account for the fluctuations in twist and also take advantage of curve-fitting techniques are under investigation.

Reversible transformations between the circle and figure-8

Reference states and transitions

The utility of dynamics in simulating large-scale configurational transitions was tested at $\Delta Lk = 1.4$, where the 1000-bp Fourier series-represented DNA exhibits three local energy minima of comparable magnitude—a circle with total energy $E = -0.1$ kcal/mol and $Wr = 0$: a figure-8 with a single point of close contact with $E = -0.1$ kcal/mol and $Wr = 1.0$; and a twist-free interwound shape with a longer zone of nonbonded contact with $E = 0.5$ kcal/mol and $Wr = 1.4$ (Liu et al., 1995). These three states, taken as representatives of the ensembles populating the various low energy wells, provide a useful framework for interpreting the configurations generated in the simulation. While the likelihood of occurrence of any one of the energy minima is close to zero (because it is only one of the many possible spatial arrangements), they act as geometric standards for identifying closely related states in the immediately surrounding potential energy wells. The circle is taken as the starting state for the calculations with γ fixed at the lower value, $5 \times 10^8\ s^{-1}$ (in physical units). Our focus here is to understand configurational transitions in a qualitative manner.

As evident from the time-dependent variations of the writhing number and principal moments in Fig. 4, *A* and *B* and selected images of the chain in Fig. 5, the DNA model undergoes dramatic configurational changes during the course of the simulation. "Circular" forms persist for ~800 iterations at the start of the simulation and later reappear for varying periods of time. These open states with writhing numbers <0.35 and third moments, $I_3 < 90$ Å, indicative of approximately planar configurations, are designated by thick line segments below the corresponding dips in *Wr* in Fig. 4 *A*. Except for the initial circular state where the first and second principal moments are equal, I_1 is always $>I_2$ (Fig. 4 *B*). Thus, the chain adopts elliptical shapes rather than a perfect circular form when the writhing number is near zero (see, for example, the image at iteration 7920 in Fig. 5). "Planar" figure-8 states with the same limits on I_3 and with *Wr* restricted to values between 0.65 and 1.35 are noted above the plotted values of the writhing number (Fig. 4 *A*). Such configurations, illustrated in Fig. 5 by the images at iterations 2000, 4340, 10,500, and 14,420, comprise >40% of the total dynamics trajectory with most cases 5–6 kcal/mol above the global energy minimum (see below). The open circles, by contrast, appear only ~10% of the time and there is a single fleeting occurrence near iteration 18,000 of a few states in the vicinity of the planar interwound minimum. The latter configurations with $Wr > 1.35$ and $I_3 < 90$ Å are highlighted by a small triangle in the upper right of Fig. 4 *A*, and illustrated by the image at iteration 17,980 in Fig. 5.

During nearly half of the simulation, the DNA exists in various nonplanar intermediate forms, some of which resemble the energy minima (such as the nonplanar interwound state at iteration 2500 illustrated in Fig. 5) and others of which appear to be high energy transition states (such as the open, globally bent configuration at iteration 12,080 in Fig. 5). While the fluctuations in writhing number, $\langle Wr\rangle = 0.7 \pm 0.3$, are comparable to those found in the simulations performed above at $\Delta Lk = 4$ with the same choice of γ, the distribution of writhing numbers cannot be fit to a single Gaussian curve. This bimodality in *Wr* is further indication of the large-scale configurational changes produced during the simulation at $\Delta Lk = 1.4$. In further contrast to the trajectory at $\Delta Lk = 4$ where the root-mean-square deviation of I_3 is small (±2 Å), the smallest principal moment undergoes much larger fluctuations at $\Delta Lk = 1.4$. The changes in I_3, 84 ± 29 Å, are markers of the opening and closing of the chain during the circle to figure-8 transitions. The mean values and root-mean-square deviations of I_1 and I_2 at $\Delta Lk = 1.4$ are, respectively, 376 ± 37 Å, 185 ± 44 Å (see Table 1 for comparison of I_1–I_3 with the related simulation at $\Delta Lk = 4$).

Energetics

Interestingly, the relative abundance of the different configurational families matches the relative order of the three minimum energy points. The much greater population of states in the vicinity of the global minimum suggests a shallower energy well surrounding the optimized figure-8 state compared to the two secondary minima. As evident from the variation of total energy in Fig. 4 *E*, most of the states generated with the Langevin protocol are much higher in energy than the minimum values. The imposed interactions of the implicit solvent environment help drive large-scale configurational transitions, but the cost is a less directed voyage about the global energy surface. The large mean potential over the dynamics simulation, $\langle E\rangle = 6.3 \pm 1.4$ kcal/mol, nevertheless provides an upper bound on the

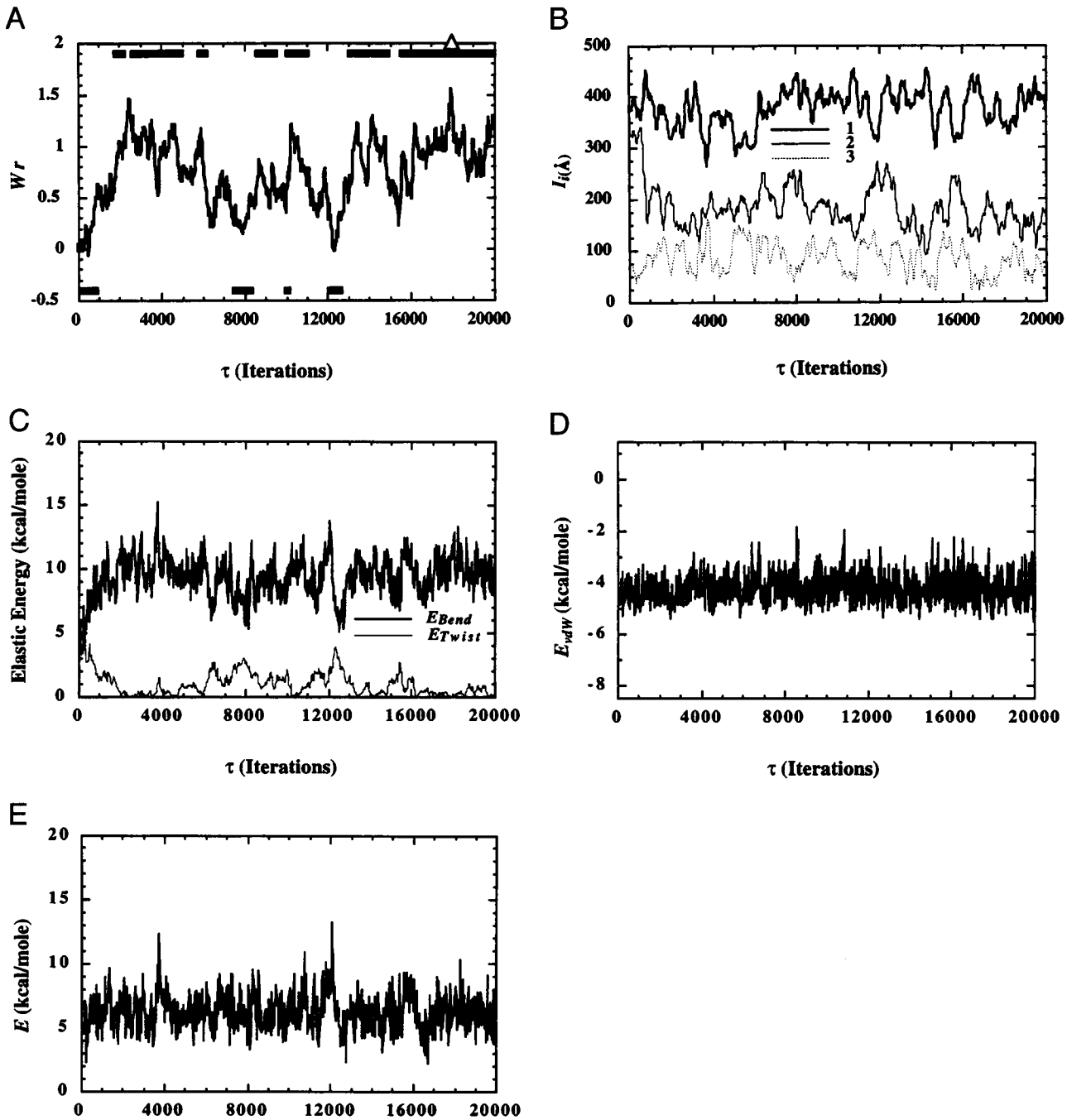

FIGURE 4 Langevin dynamics simulations of the reversible configurational transitions between circular and figure-8 states of a 1000-bp Fourier series-represented DNA supercoil. Calculations performed at $\Delta Lk = 1.4$ with $A/C = 1.0$ at the lower γ, starting from the circular equilibrium state. Evolution with time of (*A*) the writhing number (Wr), (*B*) the principal moments of the radius of gyration (I_1, I_2, I_3), (*C*) the elastic energy terms (E_{Twist}, E_{Bend}), (*D*) the van der Waals' energy (E_{vdW}), and (*E*) the total potential energy (E). Configurations with $Wr < 0.35$ and $I_3 < 90$ Å in the vicinity of the planar circle are denoted by heavy line segments in the lower half of graph (*A*); near-planar figure-8 states with $0.65 < Wr < 1.35$ and $I_3 < 90$ Å are denoted by the thick lines at the top of the figure; states with $Wr > 1.35$ and $I_3 < 90$ Å in the vicinity of the planar interwound minimum are designated by an open triangle in the upper right of (*A*).

activation energy of the transition between the circle and figure-8. The barrier impeding the interconversion is thus estimated to be no higher than 6.4 kcal/mol based on the difference between the mean potential of the dynamics simulation and the potentials of the equilibrium states (see above for numerical values).

There are significant changes in both the twisting and bending energies over the course of the simulations (Fig. 4 *C*). The twisting energy spans a narrower range of values, $\langle E_{\text{Twist}} \rangle = 1.1 \pm 0.9$ kcal/mol, than the bending contribution, $\langle E_{\text{Bend}} \rangle = 9.4 \pm 1.6$ kcal/mol, which dominates the total energy. The twisting energies are comparable to those

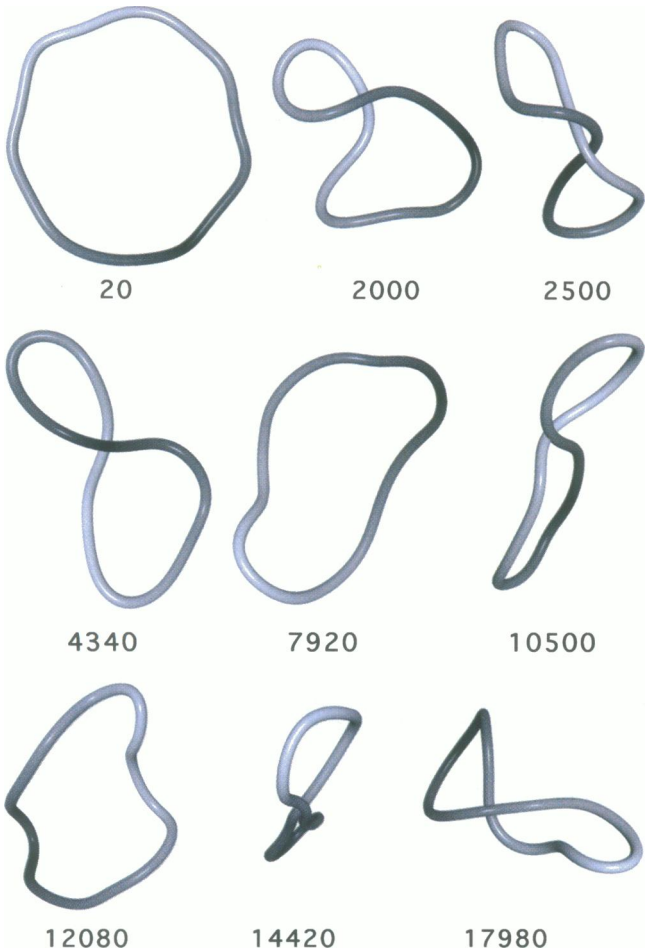

FIGURE 5 Snapshots of configurations illustrating the large-scale, reversible circle/figure-8 transitions observed in the Langevin dynamics simulations detailed in Fig. 4. The images at iterations 20 and 7920 with respective Wr, I_3 values of (0.0, 18 Å) and (0.2, 37 Å) are illustrative of the planar circular states sampled in the calculations, while those at iterations 2000, 4340, 10,500, and 14,420, where Wr, I_3 = (1.0, 51 Å), (1.0, 46 Å), (1.1, 45 Å), and (1.0, 27 Å), respectively, are typical of the configurations in the vicinity of the planar figure-8 minimum. Iteration 17,980 with Wr = 1.6, I_3 = 83 Å is representative of the few interwound forms generated in the simulations, while the configurations at iterations 2500 and 12,080, where Wr, I_3 = (1.4, 114 Å) and (0.3, 97 Å), are two of the many nonplanar states found in the calculations. Curves are shaded according to arc length to illustrate the position-independent folding and unfolding of the chain.

characterizing the global minima, but the bending terms are noticeably larger. Many of the isolated configurations include short fragments of high curvature that dissipate with time along the chain contour, much like the spreading of ripples on the surface of an agitated liquid (see Fig. 5 for examples of states with these highly curved segments). The nonbonded 6–12 term in Fig. 4 *D* also fluctuates over a limited range, $\langle E_{vdW} \rangle = -4.2 \pm 0.6$ kcal/mol, but is significantly higher in value than the attractive contributions found in the ideal figure-8, circle, and interwound minima at $\Delta Lk = 1.4$ (Liu et al., 1995). The configurations generated over most of the dynamics trajectory contain only a few points in long-range contact (see images in Fig. 5), whereas the potential energy minima generally have extended zones of interstrand association.

In addition to the large-scale changes over long time intervals, there are faster sub-fluctuations in the energy components consistent with the configurational conversions. The mean bending angles, $\langle \Delta\theta_p \rangle$, and their dispersion at representative points along the curve are nearly uniform with average values ranging between 4.3° and 5.2° and root-mean-square deviations between 2.3° and 2.6°. The chain configurations are clearly more open than those found in the corresponding $\Delta Lk = 4$ simulation, but the local fluctuations are of comparable magnitude (cf. Table 1). The fast variations in the $\langle \Delta\theta_p \rangle$ originate from unfavorable local structural changes whereas the slow fluctuations reflect global configurational changes.

Global and local motions

The global tumbling and twisting detected by the time correlations of principal axes—$C_{\cos\phi_i}, i = 1, 3$—of the supercoiled DNA at $\Delta Lk = 1.4$ are evidently slower than those found at $\Delta Lk = 4.0$ with the same value of γ (compare Fig. 6 *A* with Fig. 1 *A top*). Despite a similar rapid drop over the first 2000 iterations (roughly 20 μs), the value of $C_{\cos\phi_1}$ never attains a value of zero during the course of the simulation at $\Delta Lk = 1.4$ (Fig. 6 *A*). The large-scale changes of macromolecular shape appear to erase long-term memory of end-over-end tumbling stored in the principal axes of a more persistent global shape. The plateau in $C_{\cos\phi_1}$ over the range τ = 3000–6000 iterations reflects the slow transformations between circle and figure-8 states that occur over these time scales. Configurations separated by longer time periods tend to be of the same structural type, but with principal axes reoriented during the intervening time steps. The value of $C_{\cos\phi_1}$ decays slowly beyond this point.

The autocorrelation function of the writhing number provides an approximate estimate of the period of large-scale configurational change between the circular and figure-8 states. The small positive peaks in C_{Wr} at 3000–4000 and 6000–8000 iterations in Fig. 6 *B* roughly match the time intervals between configurational states noted in Fig. 4 *A*. The second principal moment, I_2, exhibits a similar pattern of self-correlations (Fig. 6 *C*), indicative of the connection between Wr and the macromolecular "width" measured by this parameter. The flat circular states are generally more open and expansive in terms of I_2 than the flat interwound states (see Fig. 4 *A* and *B*). The period of the writhing number is only weakly linked to the local bending angles, such as $\Delta\theta_2$, $\Delta\theta_4$, $\Delta\theta_6$, and $\Delta\theta_9$ shown in Fig. 6 *D*. The changes in the $C_{\Delta\theta_p}$, except for a rapid decrease at very short time intervals, are generally not regular; thus, there are very limited time correlations in the local bending. Some of the bending angles, however, appear to decay with the same frequency (*e.g.*, the $\Delta\theta_2$, $\Delta\theta_4$ and $\Delta\theta_6$, $\Delta\theta_9$ pairs in Fig. 6 *D*), suggesting their concerted variation during the circle-to-figure-8 transformation. The changes in the first and third

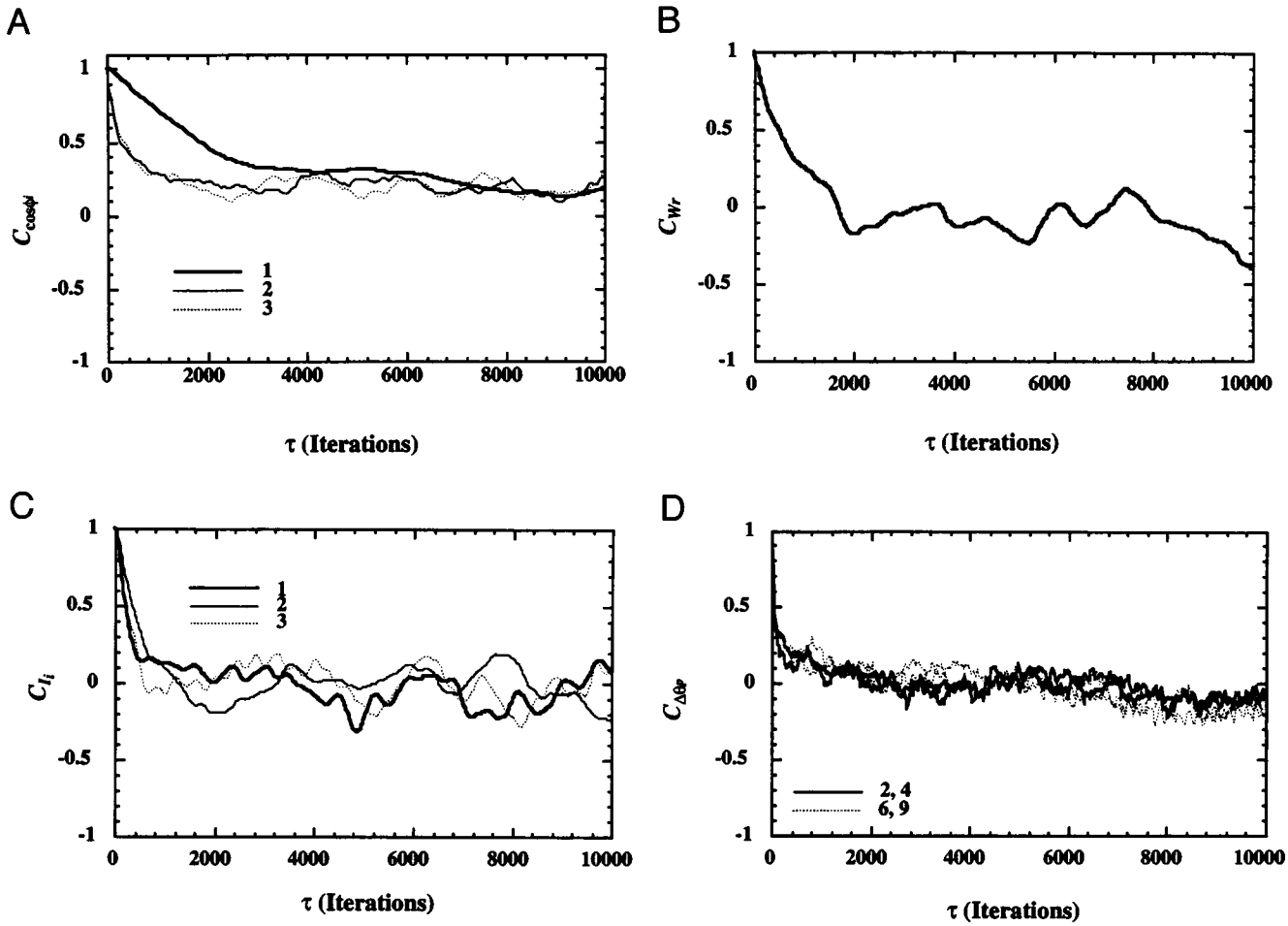

FIGURE 6 Time correlation functions of selected geometric parameters characterizing the large-scale DNA configurational transitions presented in Fig. 4. (*A*) $C_{\cos\phi_i}$, the time correlation of chain tumbling and rotation; (*B*) C_{Wr}, the autocorrelation of the writhing number; (*C*) C_{I_i}, the autocorrelation of principal moment I_i, where i = 1, 3; (*D*) $C_{\Delta\theta_p}$, the autocorrelation function of bending angle, $\Delta\theta_p$, where p = 2, 4, 6, 9. See legend to Fig. 1 and text for further details and discussion.

principal moments are also weakly coupled (Fig. 6 *C*) but are not tied to other measures of global folding. The strong interactions of imposed solvent at high γ preclude coupling between the configurational transition and the global motions of the DNA measured by the $C_{\cos\phi_i}$. The relatively weak autocorrelations of all parameters demonstrate the flexibility of DNA under the conditions of the simulation, as illustrated by the configurations in Fig. 5.

Irreversible transition from branched to interwound configurations

Branched configurations

The feasibility of simulating transitions between more widely spaced configurational states was tested at ΔLk = 4.0. There we previously identified two high-energy three-lobed minima, one with threefold symmetry and a writhing number of 2.7 and the other with twofold symmetry and Wr = 3.3 (Liu et al., 1995). The formation of the third hairpin loop in these branched states significantly increases the bending energy over that of the simple interwound energy minimum detailed in Table 1. Because of the expected dominance of the latter form, we chose to examine the interconversion between branched and interwound states of a 1000-bp elastic DNA by starting with the higher energy structure with threefold symmetry and a total energy of 11.2 kcal/mol. The results of the dynamic simulation are presented in terms of changes in the writhing number, principal moments, and energy components in Fig. 7, and selected configurations are illustrated in Fig. 8. Further details of the energies and macromolecular structures are reported in Table 2 along with corresponding parameters of the starting branched energy minimum (see Table 1 for reference energies and geometry of the interwound global energy minimum at this ΔLk). From the molecular images and the fluctuations of the principal moments (Fig. 7 *B*) and bending energy (Fig. 7 *C*), it is evident that the DNA retains a branched supercoiled shape up to iteration ~5700. The chain appears to fluctuate over the initial part of the trajectory between more extended twofold structures (such as

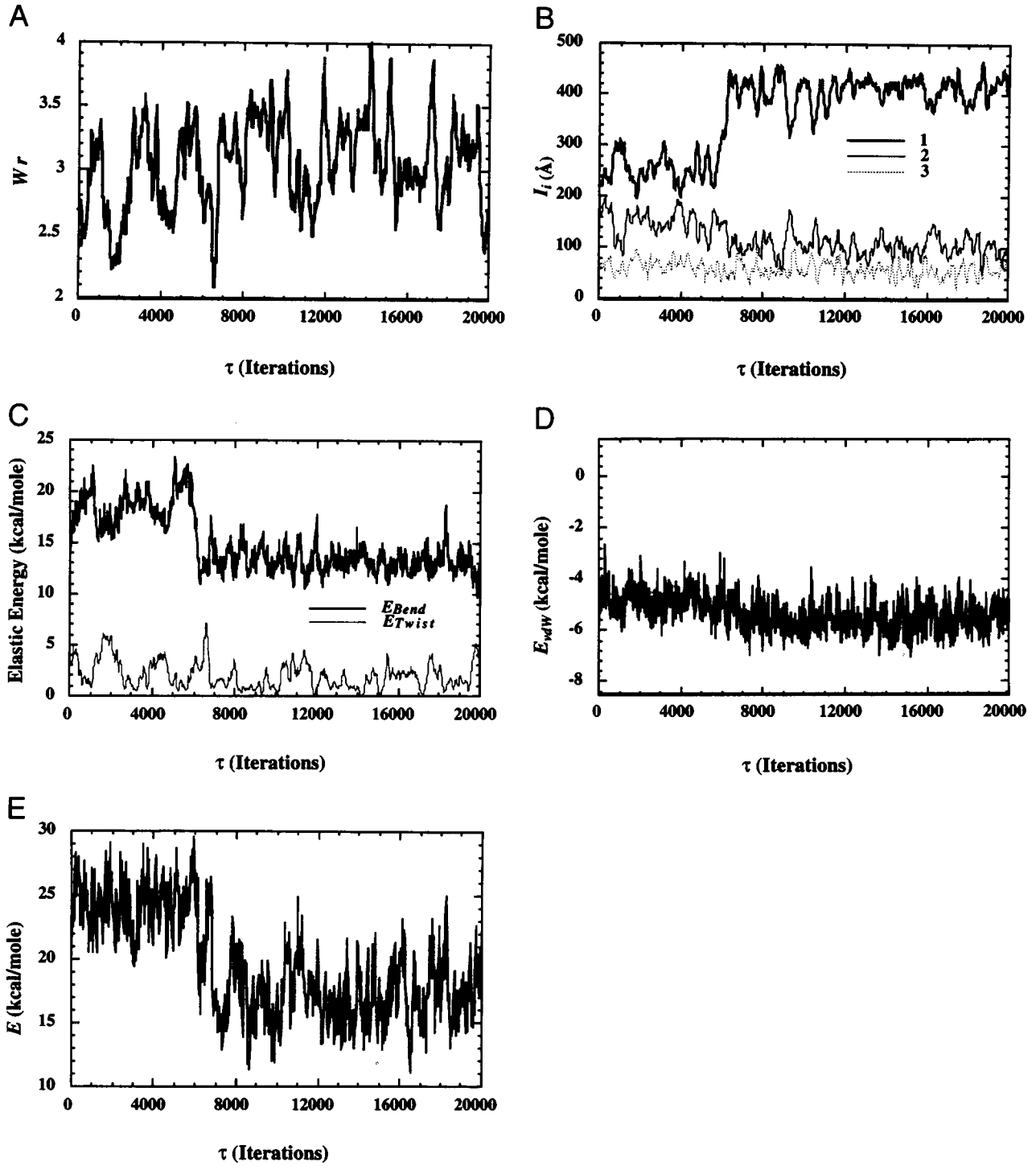

FIGURE 7 Langevin dynamics simulations of the irreversible configurational transition between three-lobed branched and linear interwound configurations of a 1000-bp Fourier series-represented DNA supercoil. Calculations performed at $\Delta Lk = 4$ with $A/C = 1.0$ at the lower γ, starting from the symmetric three-lobed, high-energy equilibrium state with $Wr = 2.7$, $E = 11.2$ kcal/mol. Evolution with time of (*A*) the writhing number (Wr), (*B*) the principal moments of the radius of gyration (I_1, I_2, I_3), (*C*) the elastic energy terms (E_{Twist}, E_{Bend}), (*D*) the van der Waals' energy (E_{vdW}), and (*E*) the total potential energy (E).

those at iterations 3200 and 5700) with I_1 near 300 Å and $E_{\text{Bend}} > 20$ kcal/mol, and threefold symmetric forms (like that at iteration 3980) with both I_1 and I_2 near 220 Å and E_{Bend} closer to 15 kcal/mol (see Fig. 8). These simulated structures also tend to be more irregular than the energy-minimized configurations (e.g., iteration 0 in Fig. 8) with the three hairpin lobes displaced out of the common plane found in the reference states.

FIGURE 8 Molecular images of selected DNA chain configurations illustrating the regular extension-compression motions of the initial three-lobed branched form and the detailed transitional pathway between branched and interwound states found in the Langevin simulations described for Fig. 7. The chain initially interconverts between threefold symmetric structures such as the starting equilibrium state and iteration 3980 and configurations with approximate twofold symmetry, illustrated by iterations 3200 and 5700. During the configurational transition, the two lobes on either side of the long axis of the twofold pseudosymmetric chain (iteration 5700) successively unfold (iteration 5800), refold (iteration 5900), and unfold (iteration 6000) before unwinding permanently (via iteration 6100) to a linear interwound configuration (iteration 6200). Curves are shaded according to arc length to illustrate relative chain movement.

TABLE 2 Comparative geometric and energetic parameters of states sampled during different stages of the Langevin dynamics simulations of an irreversible transition from branched to interwound DNA supercoils

	Branched States	Transition Zone	Interwound States	Starting Branched Configuration
τ_{Total}	5700	500	13,800	–
Wr	2.9 (0.4)	2.9 (0.2)	3.1 (0.3)	2.7
$\langle I_1 \rangle$	250 (26)	298 (30)	408 (26)	218
$\langle I_2 \rangle$	149 (25)	149 (7)	104 (20)	211
$\langle I_3 \rangle$	64 (13)	55 (12)	56 (15)	29
$\langle E_{Twist} \rangle$	2.6 (1.5)	2.4 (0.9)	1.7 (1.2)	3.3
$\langle E_{Bend} \rangle$	18.6 (1.7)	18.1 (2.6)	13.2 (1.2)	13.9
$\langle E_{vdW} \rangle$	−4.8 (0.6)	−4.7 (0.8)	−5.5 (0.6)	−6.1
$\langle E \rangle$	16.3 (1.3)	15.8 (2.1)	9.4 (1.6)	11.2
$\langle \Delta\theta_1 \rangle$	8.8 (2.7)	9.4 (3.1)	4.3 (2.2)	7.2
$\langle \Delta\theta_2 \rangle$	8.4 (2.5)	5.5 (2.7)	4.0 (2.1)	9.2
$\langle \Delta\theta_3 \rangle$	4.2 (2.3)	4.2 (2.4)	4.1 (2.1)	1.5
$\langle \Delta\theta_4 \rangle$	5.8 (3.3)	4.4 (2.3)	6.5 (3.0)	3.9
$\langle \Delta\theta_5 \rangle$	9.3 (3.1)	10.9 (2.5)	8.8 (2.8)	10.1
$\langle \Delta\theta_6 \rangle$	5.0 (2.5)	5.8 (2.6)	4.5 (2.1)	3.9
$\langle \Delta\theta_7 \rangle$	5.1 (2.2)	4.9 (2.9)	4.2 (2.2)	1.6
$\langle \Delta\theta_8 \rangle$	8.0 (2.9)	6.8 (3.0)	3.9 (2.1)	9.1
$\langle \Delta\theta_9 \rangle$	8.2 (3.5)	7.7 (3.6)	6.2 (3.0)	7.2
$\langle \Delta\theta_{10} \rangle$	3.6 (1.9)	6.6 (3.5)	8.7 (2.9)	2.7

The units of energy are kcal/mol, those of the principal moments (I_1, I_2, I_3) Ångstroms, those of the bending angles (θ_p, p = 1,10) degrees, and that of the time, τ, number of iterations. Average values and standard deviations (in parentheses) during different phases of the simulation are compared with the corresponding parameters for the three-lobed minimum energy configuration at ΔLk = 4, used as the starting point in the simulations.

Transition zone

Between iterations 5700 and 6200, the DNA converts to an interwound shape and remains in that form. It is interesting to examine this transition in more detail. The largest principal moment, I_1, rises abruptly and the bending energy drops precipitously over this range. Smaller changes are noted in the second moment, I_2, the writhing number, and the van der Waals' energy (Fig. 7). A close examination of successive images in the vicinity of the transition (Fig. 8) reveals that the lobes fold and unfold twice, forming intermediate configurations between branched and interwound forms. The transition occurs as two lobes open at their ends and one slides through the other (note the relative positioning of the shaded segments of images 5900 and 6000 in Fig. 8). The third interwound loop undergoes relatively little change during the course of conversion. Thus, two lobes of the original branched states merge during the course of the transition into a single lobe in the resulting linear structures.

Interwound configurations

The mean values of I_1, I_2, and E_{Bend} of the interwound configurations generated beyond the transition—408 ± 26 Å, 104 ± 20 Å, and 13.2 ± 1.2 kcal/mol, respectively—depart somewhat from those reported in Table 1 for interwound chains simulated with the same choice of ΔLk and γ. Re-examination of the principal moments and bending energies of the simulation reported in Figs. 1 and 2, however, reveals a slow excursion at the start of the simulation in the reverse direction from the optimized interwound reference state to a set of threefold symmetric branched configurations with $I_1 \approx I_2$ and high E_{Bend} near iteration 4500. There the branched states persist only briefly. This transformation further clarifies why the distributions of Wr in Fig. 3 are only roughly fit by simple Gaussian curves. The interwound configurations in Fig. 8, by contrast, do not return to the branched form past the transition zone at iteration 6200. The composite plots of first and second moments and bending energies in Fig. 9 not only distinguish the branched and interwound configurations but also reveal the remarkable structural similarity of the states sampled in the two simu-

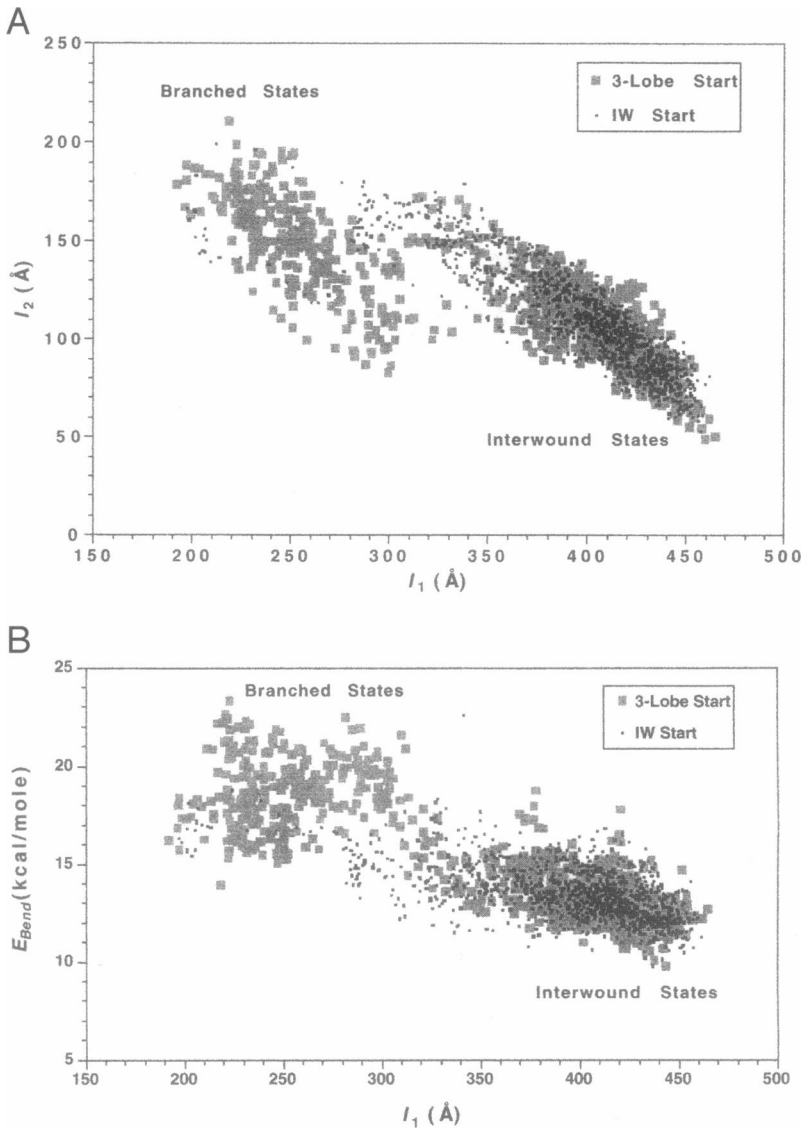

FIGURE 9 Comparative analysis of the branched and interwound states sampled in independent Langevin dynamics simulations of the $\Delta Lk = 4$ Fourier series-represented DNA chains initiated from different equilibrium states with the same γ in Figs. 1 and 7. Scatter plots of (*A*) first and second principal moments and (*B*) first moments and bending energies, the three parameters that best distinguish the two configurational families.

lations. Mean parameters of the pure interwound states generated in the earlier simulation (i.e., starting from the global energy minimum)—$\langle I_1 \rangle = 407 \pm 29$ Å, $\langle I_2 \rangle = 104 \pm 23$ Å, $\langle E_{\text{Bend}} \rangle = 13.3 \pm 1.3$ kcal/mol—are virtually indistinguishable from those derived from the corresponding data in Fig. 7 (see above). More significantly, the branched configurations that arise in the first simulation return to the linear form over virtually the same parameter space as that traversed in the simulation initiated from the branched equilibrium state. One of the three lobes disappears as its two ends move away from each other. The common pathway in this simple example demonstrates the potential utility of dynamics studies in unraveling the physicochemical mechanisms behind large-scale DNA configurational change, including those brought about by bound proteins and other ligands.

Configurational mechanism

The changes in individual bending angles provide additional insight into the mechanism of configurational transformation. The different character of the chain before, during, and after the large-scale branched to interwound configurational transition is evident from the mean values and standard deviations of $\Delta\theta_p$, $p = 1, 10$ reported in Table 2 for the three stages of the simulation. The arm containing angles $\Delta\theta_3$–$\Delta\theta_7$ persists during the entire course of the simulation with the $\Delta\theta_5$ bend centered at or near the apex of the hairpin loop and the other four bends in close contact in the adjacent interwound domain. The mean values of the five remaining bend angles—$\Delta\theta_1$, $\Delta\theta_2$, $\Delta\theta_8$–$\Delta\theta_{10}$—reveal how the two other lobes of the branched configurations deform into a single lobe in the interwound structures. The lobe initially centered in the vicinity of $\Delta\theta_1$ and $\Delta\theta_2$ completely disappears, becoming part of the interwound core during and after the transition period, while that centered originally near $\Delta\theta_8$ and $\Delta\theta_9$ shifts slightly to the neighborhood of $\Delta\theta_9$ and $\Delta\theta_{10}$. The former branch is more asymmetrically deformed than the latter in terms of mean bending within the transition zone, with the part of the loop near $\Delta\theta_1$ bent more tightly than that centered near $\Delta\theta_2$. This asymmetry appar-

ently helps to extend the interwound contact zone at $\Delta\theta_3$–$\Delta\theta_4$ and presumably facilitates the coalescence of the "intermediate" loops centered near $\Delta\theta_1$ and $\Delta\theta_9$ into the single loop found past the transition point. The fluctuations in the bending angles are relatively limited during the complete course of the simulation with the largest variations generally occurring in the vicinity of the hairpin loops. The loop "ends" are also more flexible in the simulations with the same choices of ΔLk and γ in Table 1.

As anticipated from the equilibrium structures (Liu et al., 1995), the mean value of the writhing number for the branched states in the first 5700 iterations of Fig. 7, $\langle Wr \rangle = 2.9 \pm 0.4$, is less than that for the interwound form over the remaining 13,800 iterations, $\langle Wr \rangle = 3.1 \pm 0.3$. The pathway between branched to interwound structures, however, entails a large drop in writhing number and a concomitant rise in the twisting energy (Table 2). The small decrease in the average van der Waals' energy, −4.8 kcal/mol for branched versus −5.5 kcal/mol for interwound configurations, is expected, given the added long-range contacts in the latter states. The total energy of the principal configurations is dominated by the bending contributions, with mean values of 18.6 ± 1.7 kcal/mol for the branched states and 13.2 ± 1.2 kcal/mol for the interwound forms. All three energy terms—E_B, E_T, and E_V—contribute to the potential energy within the configurational transition zone.

Global and local motions

As with the interconversion between circular and figure-8 states at $\Delta Lk = 1.4$, the transformation from branched to interwound configurations at $\Delta Lk = 4$ erases long-term memory of the global tumbling motions measured by the $C_{\cos\phi_i}$ (Fig. 10 *A*). The plateau in $C_{\cos\phi_1}$ at 0.5 over the range $\tau = 2000$–6000 iterations presumably reflects the changes in global orientation brought about by the large-scale configurational transition. Over longer time scales where pairs of configurations tend to fall into different structural families, the change in average orientation measured by $C_{\cos\phi_1}$ decreases slowly toward zero. The periodicity in $C_{\cos\phi_2}$ or $C_{\cos\phi_3}$ is different from that of $C_{\cos\phi_1}$, with both functions dropping rapidly to small values before $\tau = 1000$ iterations and then exhibiting an irregular pattern of variation.

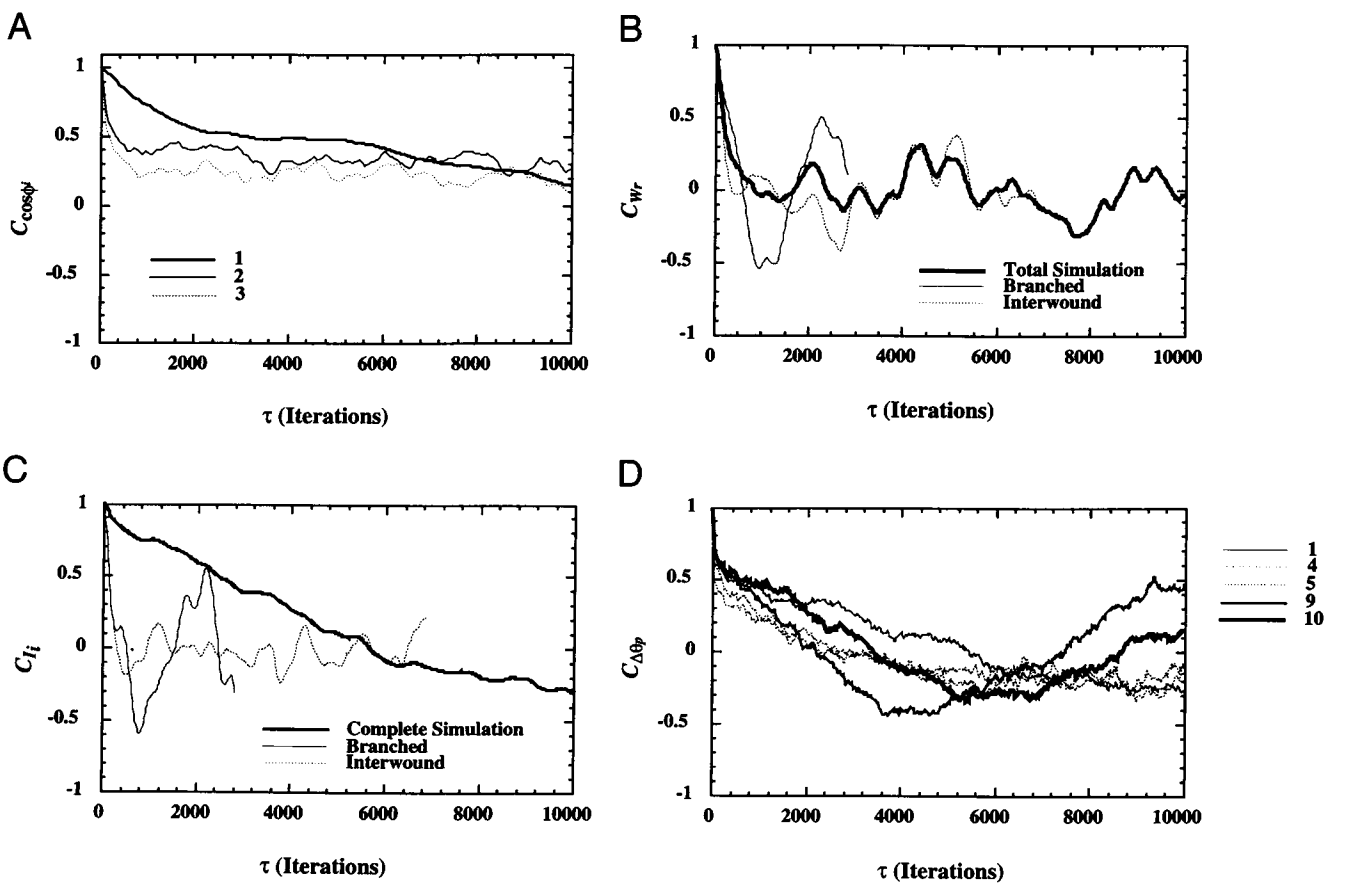

FIGURE 10 Time correlation functions of selected geometric parameters characterizing the irreversible branched to interwound DNA configurational transitions presented in Fig. 7. (*A*) $C_{\cos\phi_i}$, the time correlation of chain tumbling and rotation; (*B*) C_{Wr}, the autocorrelation of the writhing number, for individual segments—branched (*thin solid line*) and interwound (*light dotted line*)—and the complete simulation (*heavy solid line*); (*C*) C_{I_1}, the autocorrelation of the first principal moment, I_1, for individual segments and the complete simulation; (*D*) $C_{\Delta\theta_p}$, the autocorrelation function of bending angle, $\Delta\theta_p$, where $p = 1, 4, 5, 9, 10$. See legend to Fig. 1 and text for further details and discussion.

The distinct transition between branched and interwound states in these calculations makes it possible to dissect the periodic motions of the two configurational families. The plot of C_{Wr} in Fig. 10 *B* includes the autocorrelations of the writhing numbers of configurations generated before and following the large-scale structural change. The irregularity in the pattern of C_{Wr} based on the complete simulation clearly reflects the point of transition. The decreased separation between peaks in C_{Wr} before $\tau = 2500$ arises from a cancellation of branched and interwound contributions. Beyond this point, the interwound state dominates the autocorrelation function, accounting for the shorter period in C_{Wr}. This 1000-iteration repeat in C_{Wr} is also evident in the simulations starting from the interwound DNA minimum at the corresponding ΔLk in Fig. 1 *B*.

The autocorrelations of parameters, like I_1, which change dramatically during the configurational transformation, are more complex to analyze over time scales comparable to the length of time over which the two states persist. The plot of C_{I_1} at small τ in Fig. 10 *C* is not a simple composite of contributions from branched and interwound states. The large positive contributions to the autocorrelation function from states in the vicinity of the transition zone, where I_1 rises steeply, lead to the initial slow decrease in C_{I_1} computed with the data from the complete simulation. The distinctive motions of branched and linear structures are, nevertheless, apparent from the plot. The regular oscillations of the branched structures between two- and threefold symmetric forms over a 2000-iteration period are evident in the autocorrelations, as is a more rapid periodicity in I_1, associated with collective bending motions of the interwound states.

The autocorrelations of bending angles in the "unperturbed" lobe of the DNA supercoil decay very rapidly (e.g., $\Delta\theta_4$ and $\Delta\theta_5$ in Fig. 10 *D*), while parameters like $\Delta\theta_9$ and $\Delta\theta_{10}$, which undergo somewhat larger changes during the transformation from branched to interwound form, exhibit longer-range correlation. The bending measured by $\Delta\theta_1$, an angle that also changes substantially during the transition, appears to mimic the periodicity in I_1. As noted above, the initial lobe containing the $\Delta\theta_1$ bend site disappears completely in the transition from branched to interwound configurations. The incorporation of this point in the interwound contact zone accounts directly for the large increase in I_1 between the two states. The lobe containing the $\Delta\theta_9$ and $\Delta\theta_{10}$ angles simply rearranges and does not have as significant an effect on the principal moments.

DISCUSSION

Fourier series-modeled DNA

Supercoiling has critical consequences for the biological function of DNA. The very large changes in macromolecular configuration simulated in this study are important in processes such as replication, transcription, site-specific recombination, and transposition where two or more noncontiguous sites along the DNA contour come into intimate contact. The finite Fourier series representation introduced here reduces the number of independent variables needed to generate the large-scale motions of such chains while complying with the limited bending deformations of the double helix. The local structural features of a given configuration are defined in terms of the mesh points along the smooth, mathematically defined closed curve. The elastic bending is accordingly kept within the narrow bounds where the harmonic energy approximation holds. The treatment of twisting, however, is oversimplified in the present dynamics scheme. The expected time-dependent fluctuations of twist along the chain, known to be important even for the isotropic rod (Coleman et al., 1996; Tobias et al., 1996), cannot be determined on the basis of a single curve. The obvious next step is to introduce a ribbonlike representation that records both the smooth bending of the chain axis and the local helical twist. The change in orientation of sequential vectors spanning the width of the ribbon is directly related to the twisting of adjacent subunits (White, 1989). Similar treatments have been employed successfully in recent Monte Carlo and Brownian dynamics simulations of supercoiled configurational ensembles (Diekmann and Langowski, 1995; Klenin et al., 1995; Schurr et al., 1995; Chirico and Langowski, 1996; Jian, 1997; Katritch and Vologodskii, 1997). In contrast to the smooth bending model used here, the aforementioned studies define the DNA axis by a closed polygon that is subject to relatively large bending deformations at selected vertices. The deformations in twisting are correspondingly intensified at these points. In addition, it is more difficult to analyze configurational transitions in Monte Carlo or diffusive simulations.

The 1000-bp supercoiled DNA simulated at the level of controlling points in this work shows qualitative similarity to the configurational behavior of a comparably parameterized system of B-spline curves (Schlick and Olson, 1992a, b; Schlick et al., 1994b, c; Ramachandran and Schlick, 1995, 1996). Overall, the finite Fourier series tends to generate lower energy (and apparently more optimally folded) configurations than the B-spline data set. The observed differences between the two representations reflect both the global nature of the Fourier series pathway and its different control compared to the B-spline curves. Because the B-spline controlling points guide, but do not fall, along the curves which they determine, the fine tuning of overall shape is more difficult. Individual states along both simulation pathways, however, are much higher in energy that the closest minimum energy equilibrium structures.

Local versus global configurational changes

We have emphasized the connection between local and global configurational changes in supercoiled DNA. These mutual effects are most apparent in the idealized, purely elastic regime where the interactions with solvent are weak or absent (data available upon request from authors). The

end-over-end tumbling of the linear interwound DNA studied under these conditions is tied to a collective flexing motion that is linked, in turn, to the regular bending of the interwound core of the molecule. The connections are evident from the matching periodicities of the autocorrelation functions of the angles between principal axes at different time intervals, the different magnitudes of the two largest principal moments, and the variations in bending at individual points on the polymer mesh. For example, the global flexing movement that accompanies each 180° of macromolecular tumbling entails two complete cycles of chain extension and compression brought about by concerted changes in local bending angles within the intertwined contact zone of the supercoil. Furthermore, these global and local motions appear to vary independently and at a different frequency from those associated with the third principal moment, the local deformations of the two hairpin loops, and the writhing number. In other words, the bending of the interwound core of the DNA and the associated global bending and tumbling are independent of the motions of the hairpin loops and the periodic changes in *Wr*. More limited rapid fluctuations of geometric parameters and potential energy terms are superimposed on these long time-scale configurational events. The fast oscillations correspond to local conformational change that have immediate effects on the van der Waals' and bending energies.

The influence of local bending deformations on global structural change persists but gradually diminishes as the diffusive regime is explored. The solvent damps out the collective rotations of the polymer and the changes in its global shape. Still, at moderate γ, a periodicity in the writhing number of the $\Delta Lk = 4$ interwound DNA is seen and is mirrored by beats in the autocorrelation functions of specific bending angles located in the straighter and stiffer interwound segments of the polymer. Similarly, the autocorrelation patterns of the first and second principal moments can be traced to changes in bending angles at, or near, the hairpin "ends" of the elongated structure. For higher γ, no such periodicity in the writhing number is observed.

The influence of local conformation on global shape is more complicated to analyze when large-scale spatial changes occur, such as the relatively rapid conversion between circular and figure-8 forms found at $\Delta Lk = 1.4$. The large-scale variation of macromolecular shape erases long-term memory of the global rotations stored in the principal axes of a more persistent overall shape. The progress of DNA folding, as measured by the writhing number, is only weakly linked to local bending angles. Some sites of the residue bending, however, appear to decay with the same frequency, suggesting their concerted variation during the circle-to-figure-8 transformation.

Configurational variations

The 1000-bp DNA studied here spans a relatively limited range of configuration space. Despite the built-in global flexibility of the Fourier series-represented helical axis, chains with natural levels of supercoiling ($\Delta Lk = 4$) persist in linear interwound states with only a brief excursion to three-lobed arrangements. This is also found in the recent Brownian dynamics simulations of Jian (1997). By contrast, the much longer DNA molecules visualized by electron microscopy generally adopt a wide variety of branched states (Boles et al., 1990). The natural preference for such forms is expected on entropic grounds simply because there are many more possible branched configurations than simple interwound shapes. The diffusive simulations of Jian (1997) reveal the expected floppiness of interwound DNA at longer chain lengths.

Previous computational studies of chains subject to electrostatic forces (Schlick et al., 1994b) have also shown that the population of branched supercoiled arrangements will grow in longer molecules, for which the energy difference between the linear and branched states is lower. The short-range repulsive interactions between sequentially distant parts of the DNA open the interwound contact zone at the expense of increased chain bending in added interwound lobes. By contrast, the van der Waals' term introduced in this study to mimic, in addition to repulsion, attractive interactions between closely spaced charged rods at high salt concentrations (Odijk, 1994; Ray and Manning, 1994; Wissenburg et al., 1994) helps stabilize extended, tightly associated interwound shapes. The attractive contributions are less important in the present simulations at low imposed supercoiling ($\Delta Lk = 1.4$) where the chain freely interconverts between circular and figure-8 states with few points in close contact. The van der Waals' term, however, appears to restrict the slithering of the chain at both levels of supercoiling (note the limited intramolecular migration of contour-shaded images in Figs. 2, 5, and 8). The mutual passage of chain segments is more significant in Langevin dynamics simulations that incorporate electrostatic interactions (Schlick et al., 1994b) and in molecular dynamics simulations subject to a hard-core (Heaviside step) potential (Sprous and Harvey, 1996; Tan et al., 1996).

The limited global mobility of the DNA translates at the local level into restricted residue bending. The root-mean-square bending fluctuations of the most flexible set of dynamics trajectories are only a fraction of the angular deformations expected from the assumed bending constant. Supercoiled configurations collected in Monte Carlo sampling based on a similar elastic potential (Klenin et al., 1991) are much more irregular than those found here, most likely due to the large global moves introduced in the sampling protocol. Our omission of energy contributions arising from the instantaneous deviations of the twist angle may account, in part, for the limited range of local chain bending. The macroscopic modeling of the DNA by a compact, curve-fitting representation may be another factor. Incorporation of torsional forces, in particular, significantly broadens the configurational profiles generated in recent Brownian dynamics simulations of supercoiled DNA (Chirico, 1996). Finer models of DNA are still many years

away, as current all-atom simulations are limited to dozens of residues. The picture of supercoiled DNA in solution is expected to be diverse and dynamic with the coexistence and constant interconversion of different interwound and branched configurations. Hydrodynamic interactions neglected in the present treatment are also important to consider.

G. L. is grateful to Hoffmann-La Roche, Inc. for tuition assistance. Computations were performed at the Rutgers University Center for Computational Chemistry and at New York University. T. S. is an investigator at the Howard Hughes Medical Institute.

This research was generously supported by U.S. Public Health Service Research Grant GM 34809 and Parallel Computing Resource for Structural Biology Grant RR08102, the National Science Foundation (Grand Challenge Award ASC 9318159), and the Alfred P. Sloan Foundation.

REFERENCES

Allison, S. A., and J. A. McCammon. 1984. Transport properties of rigid and flexible macromolecules by Brownian dynamics simulation. *Biopolymers*. 23:167–187.

Bauer, W. R. 1978. Structure and reactions of closed duplex DNA. *Annu. Rev. Biophys. Bioeng.* 7:287–313.

Bednar, J., P. Furrer, V. Katritch, A. Z. Stasiak, J. Dubochet, and A. Stasiak. 1995. Determination of DNA persistence length by cryo-electron microscopy. Separation of the static and dynamic contributions to the apparent persistence length of DNA. *J. Mol. Biol.* 254:579–594.

Bednar, J., P. Furrer, A. Stasiak, J. Dubochet, E. H. Egelman, and A. D. Bates. 1994. The twist, writhe, and overall shape of supercoiled DNA change during counterion-induced transition from a loosely to a tightly interwound superhelix. Possible implications for DNA structure in vivo. *J. Mol. Biol.* 235:825–847.

Bensimon, D. 1996. Force: a new structural control parameter? *Structure*. 4:885–889.

Bensimon, A., A. Simon, A. Chiffaudel, V. Croquette, F. Heslot, and D. Bensimon. 1994. Alignment and sensitive detection of DNA by a moving interface. *Science*. 265:2096–2098.

Bloomfield, V. A., R. W. Wilson, and D. C. Rau. 1980. Polyelectrolyte effects in DNA condensation by polyamines. *Biophys. Chem.* 11: 339–343.

Boles, C. D., J. H. White, and N. R. Cozzarelli. 1990. Structure of plectonemically supercoiled DNA. *J. Mol. Biol.* 213:931–951.

Chandler, D. 1987. Introduction to Modern Statistical Mechanics. Chap. 8. Oxford University Press, New York.

Cheatham, T. E. III, and P. A. Kollman. 1996. Observation of the A-DNA to B-DNA transition during unrestrained molecular dynamics in aqueous solution. *J. Mol. Biol.* 259:434–444.

Chirico, G. 1996. Torsional-bending infinitesimal dynamics of a DNA chain. *Biopolymers*. 38:801–811.

Chirico, G., and J. Langowski. 1991. Calculating hydrodynamics properties of DNA through a second-order Brownian dynamics algorithm. *J. Chim. Phys.* 88:2561–2566.

Chirico, G., and J. Langowski. 1992. Calculating hydrodynamic properties of DNA through a second-order Brownian dynamics algorithm. *Macromolecules*. 25:769–775.

Chirico, G., and J. Langowski. 1994. Kinetics of DNA supercoiling studied by Brownian dynamics simulation. *Biopolymers*. 34:415–433.

Chirico, G., and J. Langowski. 1996. Brownian dynamics simulations of supercoiled DNA with bent sequences. *Biophys. J.* 71:955–971.

Cluzel, P., A. Lebrun, C. Heller, R. Lavery, J.-L. Viovy, D. Chatenay, and F. Caron. 1996. DNA: an extensible molecule. *Science*. 271:792–794.

Coleman, B. D., M. Lembo, and I. Tobias. 1996. A new class of flexure-free torsional vibrations of annular rods. *Meccanica*. 31:565–575.

Crothers, D. M., J. Drak, J. D. Kahn, and S. D. Levene. 1992. DNA bending, flexibility, and helical repeat by cyclization kinetics. *Methods Enzymol.* 212:3–29.

Diekmann, S., and J. Langowski. 1995. Supercoiling couples DNA curvature to the overall shape and the internal motion of the DNA molecule in solution. *J. Mol. Struct.* 336:227–234.

Dunn, T. M., S. Hahn, S. Ogden, and R. F. Schleif. 1984. An operator at −280 bp that is required for repression of *ara*BAD operon promoter: addition of DNA helical turns between the operator and promoter cyclically hinders repression. *Proc. Natl. Acad. Sci. USA*. 81:5017–5020.

Eisenberg, H. 1987. DNA flexing, folding, and function. *Accts. Chem. Res.* 20:276–282.

Elcock, A. H., and J. A. McCammon. 1995. Sequence dependent hydration of DNA: theoretical results. *J. Am. Chem. Soc.* 117:10161–10162.

Fenley, M. O., W. K. Olson, I. Tobias, and G. S. Manning. 1994. Electrostatic effects in short superhelical DNA. *Biophys. Chem.* 50:255–271.

Flory, P. J. 1969. Statistical Mechanics of Chain Molecules. Chap. 4. Interscience, New York.

Fuller, F. B. 1971. The writhing number of a space curve. *Proc. Natl. Acad. Sci. USA*. 68:815–819.

Fuller, F. B. 1978. Decomposition of the linking number of a closed ribbon: a problem from molecular biology. *Proc. Natl. Acad. Sci. USA*. 75:3557–3661.

Gebe, J. A., S. A. Allison, J. B. Clendenning, and J. M. Schurr. 1995. Monte Carlo simulations of supercoiling free energies for unknotted and trefoil knotted DNAs. *Biophys. J.* 68:619–633.

Gellert, M., and H. A. Nash. 1987. Communication between segments of DNA during site-specific recombination. *Nature*. 401–404.

Germond, J. E., B. Hirt, P. Oudet, M. Gross-Bellard, and P. Chambon. 1975. Folding of the DNA double helix in chromatin-like structures from simian virus 40. *Proc. Natl. Acad. Sci. USA*. 72:1843–1847.

Gordon, W. J., and R. E. Riesenfeld. 1974. B-spline curves and surfaces. *In* Computer Aided Geometric Design. R. E. Barnhill and R. E. Riesenfeld, editors. Academic Press, New York. 95–126.

Gorin, A. A., V. B. Zhurkin, and W. K. Olson. 1995. B-DNA twisting correlates with basepair morphology. *J. Mol. Biol.* 247:34–48.

Griffith, J., A. Hochschild, and M. Ptashne. 1986. DNA loops induced by cooperative binding of λ repressor. *Nature*. 322:750–752.

Hagerman, P. J. 1985. Analysis of the ring-closure probabilities of isotropic wormlike chains: application to duplex DNA. *Biopolymers*. 24: 1881–1897.

Hagerman, P. J. 1988. Flexibility of DNA. *Annu. Rev. Biophys. Biophys. Chem.* 17:265–286.

Hansma, H. G., I. Revenko, K. Kim, and D. E. Laney. 1996. Atomic force microscopy of long and short double-stranded, single-stranded and triple-stranded nucleic acids. *Nucleic Acids Res.* 24:713–720.

Hao, M.-H., and W. K. Olson. 1989a. Modeling DNA supercoils and knots with B-spline functions. *Biopolymers*. 28:873–900.

Hao, M.-H., and W. K. Olson. 1989b. Searching the global equilibrium configurations of supercoiled DNA by simulated annealing. *Macromolecules*. 22:3292–3303.

Heath, P. J., J. B. Clendenning, B. S. Fujimoto, and J. M. Schurr. 1996. Effect of bending strain on the torsion elastic constant of DNA. *J. Mol. Biol.* 260:718–730.

Heichman, K. A., and R. C. Johnson. 1990. The Hin invertasome: protein-mediated joining of distance recombination sites at the enhancer. *Science*. 249:511–517.

Irani, M. H., L. Orosz, and S. Adhya. 1983. A control element within a structural gene: the *gal* operon of Escherichia coli. *Cell*. 32:783–788.

Jian, H. 1997. A combined wormlike-chain and bead model for dynamic simulations of long DNA. Ph.D. Thesis, New York University, New York.

Jian, H., A. V. Vologodskii, and T. Schlick. 1997. A combined wormlike-chain and bead model for dynamic simulations of long DNA. *J. Comp. Phys.* 136. In press.

Kanaar, R., A. Klippel, E. Shekhtman, J. M. Dungan, R. Kahmann, and N. Cozzarelli. 1990. Processive recombination by the phage Mu Gin system; implications for the mechanisms of DNA strand exchange, DNA site alignment, and enhancer action. *Cell*. 62:353–366.

Katritch, V., and A. V. Vologodskii. 1997. The effect of intrinsic curvature on conformational properties of circular DNA. *Biophys. J.* 72: 1070–1079.

Klenin, K. V., M. D. Frank-Kamenetskii, and J. Langowski. 1995. Modulation of intramolecular interactions in superhelical DNA by curved sequences. A Monte-Carlo simulation study. *Biophys. J.* 68:81–88.

Klenin, K. V., A. V. Vologodskii, V. V. Anshelevich, A. M. Dykhne, and M. D. Frank-Kamenetskii. 1991. Computer simulation of DNA supercoiling. *J. Mol. Biol.* 217:413–419.

Kuhn, W. 1936. Beziehungen zwischen Molekülgrösse, statistischer Molekülgestalt und elastischen Eigenschaften hochpolymerer Stoffe. *Kolloid Z.* 76:258–271.

Kuhn, W. 1939. Molekülkonstellation und Kristallitorientierung als Ursachen kautschukähnlicher Elastizität. *Kolloid Z.* 87:3–12.

Landau, L. D., and E. M. Lifshitz. 1980. Statistical Physics, 3rd Ed., Part 1. Pergamon Press, Oxford. 396–400.

Le Bret, M. 1978. Relationship between the energy of superhelix formation, the shear modulus, and the torsional Brownian motion of DNA. *Biopolymers.* 17:1939–1955.

Le Bret, M. 1980. Monte Carlo computation of the supercoiling energy, the sedimentation constant, and the radius of gyration of unknotted and knotted circular DNA. *Biopolymers.* 19:619–637.

Le Bret, M. 1984. Twist and writhing in short circular DNAs according to first-order elasticity. *Biopolymers.* 23:1835–1867.

Levene, S. D., and D. M. Crothers. 1986. Ring closure probabilities for DNA fragments by Monte Carlo simulation. *J. Mol. Biol.* 189:61–72.

Lewis, M., G. Chang, N. C. Horton, M. A. Kercher, H. C. Pace, M. A. Schumacher, R. G. Brennan, and P. Lu. 1996. Crystal structure of the lactose operon repressor and its complexes with DNA and inducer. *Science.* 271:1247–1254.

Liu, G.-H., W. K. Olson, and T. Schlick. 1995. Application of Fourier methods to computer simulation of supercoiled DNA. *Comp. Polymer Sci.* 5:7–27.

Loncharich, R. J., B. R. Brooks, and R. W. Pastor. 1992. Langevin dynamics of peptides: the frictional dependence of isomerization rates of *N*-acetylalanyl-*N'*-methylamide. *Biopolymers.* 32:523–535.

Lyubchenko, Y. L., and L. S. Shlyakhtenko. 1997. Visualization of supercoiled DNA with atomic force microscopy in situ. *Proc. Natl. Acad. Sci. USA.* 94:496–501.

Marky, N. L., and W. K. Olson. 1994. Spatial translational motions of the basepairs in DNA molecules: applications of the extended matrix generator method. *Biopolymers.* 34:121–142.

Maroun, R. C., and W. K. Olson. 1988. Base sequence effects in double helical DNA. II. Configurational statistics of rodlike chains. *Biopolymers.* 27:561–584.

Matsumoto, M., and K. Doi. 1994. Brownian dynamics simulation of DNA gel electrophoresis. *Mol. Simulation.* 12:219–226.

McCammon, J. A., and S. C. Harvey. 1987. Dynamics of Proteins and Nucleic Acids, Chap. 3. Cambridge University Press, Cambridge.

McConnell, K. J., R. Nirmala, M. A. Young, G. Ravishanker, and D. L. Beveridge. 1994. A nanosecond molecular dynamics trajectory for a B DNA double helix: evidence for substates. *J. Am. Chem. Soc.* 116: 4461–4462.

Moitoso de Vargas, L., S. Kim, and A. Landy. 1989. DNA looping generated by DNA bending protein IHF and the two domains of lambda integrase. *Science.* 244:1457–1461.

Nie, S., D. T. Chiu, and R. N. Zare. 1995. Real-time detection of single molecules in solution by confocal fluorescence microscopy. *Anal. Chem.* 67:2849–2857.

Odijk, T. 1994. Long-range attraction in polyelectrolyte solutions. *Macromolecules.* 27:4998–5003.

Olson, W. K. 1979. The flexible DNA helix. II. Superhelix formation. *Biopolymers.* 18:1235–1260.

Olson, W. K. 1996. Simulating DNA at low resolution. *Curr. Opin. Struct. Biol.* 6:242–256.

Olson, W. K., M. S. Babcock, A. Gorin, G.-H. Liu, N. L. Marky, J. A. Martino, S. C. Pedersen, A. R. Srinivasan, I. Tobias, T. P. Westcott, and P.-S. Zhang. 1995. Flexing and folding double helical DNA. *Biophys. Chem.* 55:7–29.

Olson, W. K., N. L. Marky, R. L. Jernigan, and V. B. Zhurkin. 1993. Influence of fluctuations on DNA curvature. A comparison of flexible and static wedge models of intrinsically bent DNA. *J. Mol. Biol.* 232: 530–554.

Olson, W. K., and P. Zhang. 1991. Computer simulation of DNA supercoiling. *Methods Enzymol.* 203:403–432.

Perkins, T. T., D. E. Smith, and S. Chu. 1994. Direct observation of tube-like motion of a single polymer chain. *Science.* 264:819–826.

Podgornik, R., H. H. Strey, D. C. Rau, and V. A. Parsegian. 1995. Watching molecules crowd: DNA double helices under osmotic stress. *Biophys. Chem.* 57:111–121.

Ptashne, M. 1986. Gene regulation by proteins acting nearby and at a distance. *Nature.* 322:697–701.

Ramachandran, G., and T. Schlick. 1995. Solvent effects on supercoiled DNA dynamics explored by Langevin dynamics simulation. *Physiol. Rev. E, part B* 5:6188–6203.

Ramachandran, G., and T. Schlick. 1996. Beyond optimization, simulating the dynamics of supercoiled DNA by a macroscopic model. *In* DIMACS Series in Discrete Mathematics and Theoretical Computer Science. P. Pardalos and D. Shalloway, editors. American Math. Society, Providence, RI, 215–231.

Ray, J., and G. S. Manning. 1994. An attractive force between two rodlike polyions mediated by the sharing of condensed counterions. *Langmuir.* 10:2450–2461.

Samori, B., C. Nigro, A. Gordano, I. Muzzalupo, and C. Quagliariello. 1996. Trapping and imaging molecular dynamics by combining scanning force microscopy with topology. *Angew. Chem. Int. Ed. Engl.* 35:529–530.

Schellman, J. A., and S. C. Harvey. 1995. Static contributions to the persistence length of DNA and dynamics contributions to DNA curvature. *Biophys. Chem.* 55:95–114.

Schlick, T. 1995. Modeling superhelical DNA: recent analytical and dynamical approaches. *Curr. Opin. Struct. Biol.* 5:245–262.

Schlick, T., and A. Fogelson. 1992a. TNPACK—a truncated Newton minimization package for large-scale problems. I. Algorithm and usage. *ACM Trans. Math. Softw.* 18:46–70.

Schlick, T., and A. Fogelson. 1992b. TNPACK—a truncated Newton minimization package for large-scale problems. II. Implementation examples. *ACM Trans. Math. Softw.* 18:71–111.

Schlick, T., B. Li, and M.-H. Hao. 1994a. Calibration of the timestep for molecular dynamics of supercoiled DNA modeled by B-spline. *In* Structure Biology: State of the Art. R. H. Sarma and M. H. Sarma, editors. Adenine Press, Schenectady, NY, 157–174.

Schlick, T., B. Li, and W. K. Olson. 1994b. The influence of salt on the structure and energetics of supercoiled DNA. *Biophys. J.* 67:2146–2166.

Schlick, T., and W. K. Olson. 1992a. Supercoiled DNA energetics and dynamics by computer simulation. *J. Mol. Biol.* 223:1089–1119.

Schlick, T., and W. K. Olson. 1992b. Trefoil knotting revealed by molecular dynamics simulations of supercoiled DNA. *Science.* 257: 1110–1115.

Schlick, T., W. K. Olson, T. Westcott, and J. P. Greenberg. 1994c. On higher buckling transitions in supercoiled DNA. *Biopolymers.* 34: 565–597.

Schurr, J. M., H. P. Babcock, and J. A. Gebe. 1995. Effect of anisotropy of the bending rigidity on the supercoiling free energy of small circular DNAs. *Biopolymers.* 36:633–641.

Smith, S. B., Y. Cui, and C. Bustamante. 1996. Overstretching B-DNA: the elastic response of individual double-stranded and single-stranded DNA molecules. *Science.* 271:795–799.

Sprous, D., and S. C. Harvey. 1996. Action at a distance: effects of sequence on slither, branching, and intramolecular concentration. *Biophys. J.* 69:1903–1908.

Sprous, D., R. K.-Z. Tan, and S. C. Harvey. 1996. Molecular modeling of closed circular DNA thermodynamic ensembles. *Biopolymers.* 38: 243–258.

Strick, T. R., J.-F. Allemand, D. Bensimon, A. Bensimon, and V. Croquette. 1996. The elasticity of a single supercoiled DNA molecule. *Science.* 271:1835–1837.

Tan, R. K.-Z., and S. C. Harvey. 1990. Succinct macromolecular models: application to supercoiled DNA. *In* Theoretical Biochemistry and Molecular Biophysics, Vol. 1: DNA. D. L. Beveridge and R. Lavery, editors. Adenine Press, Schenectady, NY, 125–137.

Tan, R. K.-Z., D. Sprous, and S. C. Harvey. 1996. Molecular dynamics simulations of small DNA plasmids: effects of sequence and supercoiling on intramolecular motions. *Biopolymers*. 38:259–278.

Taylor, W. H., and P. J. Hagerman. 1990. Application of the method of phage T4 DNA ligase-catalyzed ring-closure to the study of DNA structure. II. NaCl-dependence of DNA flexibility and helical repeat. *J. Mol. Biol.* 212:363–376.

Timsit, Y., and D. Moras. 1994. DNA self-fitting: the double helix directs the geometry of its supramolecular assembly. *EMBO J.* 13:2737–2746.

Timsit, Y., and D. Moras. 1995. Self-fitting and self-modifying properties of the B-DNA molecule. *J. Mol. Biol.* 251:629–647.

Tobias, I., B. D. Coleman, and M. Lembo. 1996. A class of exact dynamical solutions in the elastic rod model of DNA with implications for the theory of fluctuations in the torsional motion of plasmids. *J. Chem. Phys.* 105:2517–2526.

van Waveren, M., M. Bishop, and J. P. J. Michels. 1988. Brownian dynamics study of the relaxation behabior of linear and ring polymers. *J. Chem. Phys.* 88:1326–1327.

Volkmuth, W. D., T. Duke, R. H. Austin, and E. C. Cox. 1995. Trapping of branched DNA in microfabricated structures. *Proc. Natl. Acad. Sci. USA.* 92:6887–6891.

Vologodskii, A. V., and N. R. Cozzarelli. 1994. Supercoiling, knotting, looping and other large-scale conformational properties of DNA. *Curr. Opin. Struct. Biol.* 4:372–375.

Vologodskii, A. V., S. D. Levene, M. D. Frank-Kamenetskii, and N. R. Cozzarelli. 1992. Conformational and thermodynamic properties of supercoiled DNA. *J. Mol. Biol.* 227:1224–1243.

Westcott, T. P. 1996. Elasticity theory and numerical analysis of DNA supercoiling. Ph.D. Thesis, Rutgers, the State University of New Jersey, New Brunswick, NJ.

Westcott, T. P., I. Tobias, and W. K. Olson. 1997. Modeling self-contact forces in the elastic theory of DNA supercoiling. *J. Chem. Phys.* 107: 3967–3980.

White, J. H. 1969. Self-linking and the Gauss integral in higher dimensions. *Am. J. Math.* 91:693–728.

White, J. H. 1989. An introduction to the geometry and topology of DNA structure. *In* Mathematical Methods for DNA Sequences. M. S. Waterman, editor. CRC Press, Boca Raton, FL, 225–253.

Wissenburg, P., T. Odijk, P. Cirkel, and M. Mandel. 1994. Multimolecular aggregation in concentrated isotropic solutions of mononucleosomal DNA in 1 M sodium chloride. *Macromolecules*. 27:306–308.

Yang, L. Q., and B. M. Pettitt. 1996. B to A transition of DNA on the nanosecond time scale. *J. Phys. Chem.* 100:2564–2566.

Yevich, R., and W. K. Olson. 1979. The spatial distributions of randomly coiling polynucleotides. *Biopolymers*. 18:113–145.

Yin, H., M. D. Wang, K. Svoboda, R. Landick, S. M. Block, and J. Gelles. 1995. Transcription against an applied force. *Science*. 270:1653–1658.

York, D. M., W. Yang, H. Lee, T. Darden, and L. G. Pedersen. 1995. Toward the accurate modeling of DNA: the importance of long-range electrostatics. *J. Am. Chem. Soc.* 117:5001–5002.

Yoshikawa, K., and Y. Matsuzawa. 1995. Discrete phase transition of giant DNA dynamics of globule formation from a single molecular chain. *Physica D.* 84:220–227.

Zajac, E. E. 1962. Stability of two planar loop elasticas. *Trans. ASME, Ser. E, J. Appl. Mech.* 29:136–142.

Zhang, P., W. K. Olson, and I. Tobias. 1991. Accelerated record keeping Fourier series Monte Carlo simulations of an isotropic elastic rod model of DNA. *Comp. Polymer Sci.* 1:3–17.

Zhang, P., I. Tobias, and W. K. Olson. 1994. Computer simulation of protein-induced structural changes in closed circular DNA. *J. Mol. Biol.* 242:271–290.

Zhurkin, V. B., N. B. Ulyanov, A. A. Gorin, and R. L. Jernigan. 1991. Static and statistical bending of DNA evaluated by Monte Carlo simulations. *Proc. Natl. Acad. Sci. USA.* 88:7046–7050.

Zivanovic, Y., I. Goulet, B. Révet, M. L. Bret, and A. Prunell. 1988. Chromatin reconstitution on small DNA rings II. DNA supercoiling on the nucleosome. *J. Mol. Biol.* 200:267–290.